AD NUMBER

AD816316

NEW LIMITATION CHANGE

TO

Approved for public release, distribution unlimited

FROM

Distribution authorized to U.S. Gov't. agencies and their contractors; Administrative/Operational Use; MAY 1967. Other requests shall be referred to Office of Naval Research, 800 North Quincy Street, Arlington, VA 22217-5660.

AUTHORITY

ONR Notice, 27 Jul 1971

AD 816316

THIRD SUMMARY REPORT

ON

STRUCTURAL STUDIES OF BEARING STEEL

UNDERGOING CYCLIC STRESSING

May 20, 1967

Contributors

J. A. Martin, S.F.Borgese,

A. D. Eberhardt

Project Leader: J A Martin

Approved : G H Bailey

Released : [illegible]

NR259-055/11-29-65

ONR Contract No. Nonr-4433 (00)

SKF Report AL67M050

SKF Code 6271-6819

SKF Project 10-3

SKF Reg. 610 119
610 13

SPONSORED BY:
U.S. DEPARTMENT OF THE NAVY
OFFICE OF NAVAL RESEARCH
DIRECTOR, SURFACE & AMPHIBIOUS PROGRAMS
NAVAL APPLICATIONS GROUP
WASHINGTON 25, D.C.

RESEARCH LABORATORY

SKF INDUSTRIES, INC.

ENGINEERING AND RESEARCH CENTER

KING OF PRUSSIA, PA.

Reproduction in whole or part is permitted for any purpose of the United States Government. Since this is an interim Summary Report, the information herein is tentative and subject to changes, corrections, and modifications".

TABLE OF CONTENTS

TABLE OF CONTENTS (CONT'D)

LIST OF TABLES

LIST OF ENCLOSURES

LIST OF ENCLOSURES (CONT'D)

LIST OF ENCLOSURES (CONT'D)

AL67M050

STRUCTURAL STUDIES OF BEARING STEEL

UNDERGOING CYCLIC STRESSING

SUMMARY

A metallurgical investigation of the failure mechanisms which operate in bearing steels during cyclic stressing in rolling contact has been in progress since March 1, 1964 under Contract Nonr 4433(00).

Results of this program have been reported in previous Summary Reports (1)*, (2); three Progress Reports (3), (4), (5), and in a published paper (6).

The present report is written in 5 parts.

Part I presents the concepts of microstructural changes which accompany fatigue. This section reviews previously reported findings made regarding the nature and physical descriptions of the deformation bands which develop in bearing steels during cyclic stressing in rolling contact. Current findings of an electron transmission microscope tempering study of deformation bands are summarized. This study will be presented in full detail in Special Report AL67M051 to be issued shortly.

Part II deals with the identification of failure initiation points by observations of deformation bands and shows how they can be used as an indicator of the severity of defects. The initiation of fatigue failures at various types of surface defects is described and documented.

---

*Numbers in parenthesis refer to the list of references at the end of this report.

Part III describes the appearance of different types of surface originated fatigue failures and presents data showing the relative frequency of failures, identified as surface originated, in recent endurance test experience. The appearance of subsurface initiated spalls is also examined and a brief description is given of the crack propagation mechanisms observed in spalls by electron fractographic techniques. Full details of the electron fractographic techniques and results are given in Special Report AL67M060, to be issued shortly.

Part IV discusses the role of deformation bands in the propagation of cracks.

Part V is a discussion of results, which summarizes the important conclusions and lays the basis for future work.

DETAILS

PART I-STRUCTURAL ALTERATIONS IN FATIGUE

Structural alterations occurring during cyclic stressing are well established phenomena that have been observed in a variety of materials. Under electron microscope observation of thin foils, alterations are sometimes seen as dislocation sub-structures (7),(8),(9) which, from their appearance, are best described as cellular. Any type of structural alteration requiring the re-arrangement of dislocations is, by definition, a plastic disturbance. Many of the microstructural changes associated with fatigue that are described in the literature are manifestations of plastic flow. On the electron microscope scale of observation these include the cell structures described above. On the light microscope scale, the intrusions and extrusions reported by Forsyth (10) and the slip bands, notches and fissures described by Wood (11) are plastic flow phenomena.

There are also other types of fatigue related microstructural changes that are not plastic phenomena. These are diffusion induced changes where, according to Wood (11)"impurities and alloying elements, by diffusing to the deformation zones may alter the local structure".

In the course of the present program both types of micro-structural change have been seen. The development of a white etching structural alteration in hardened bearing steels with prolonged rolling contact cycling of bearing elements has been described in the previous reports (1-6). On closer examination the white etching areas are frequently found to be bordered by large "lenticular" carbides, so called since in a three dimensional view they tend to be somewhat lens shaped.

Enclosure 1 shows some typical "white areas" with large lenticular carbides. These surrounding carbides clearly are the result of diffusion processes since they are many magnitudes larger than any other carbides in the structure, and they could not have been formed by purely mechanical rearrangement of carbides. The original carbides which remained undissolved during austenitizing can barely be resolved at the magnification shown (2000X).

Further evidence for the formation of lenticular carbides by carbon migration is given by the two tempering experiments described below.

Enclosure 2 summarizes the findings of a light microscope study where the same deformation bands are shown before and after tempering. The specimen used was taken from an endurance tested bearing that had been specially heat treated by a double austenitizing and quench procedure in order to produce an exceptionally fine carbide structure. This structure makes it possible to detect local variations in carbide content, after tempering, by comparing the level of blackening caused by precipitation of small carbides.

After tempering at 500°C for 1 hour most of the carbon in solid solution has precipitated and it is apparent that the overall carbon content within the white area is lower than that of the undisturbed material. Only carbon migration away from the white area towards the lenticular carbides can account for this difference.

A more detailed study has been conducted by tempering thin foil specimens containing deformation bands in the electron microscope. This study, described fully in Special Report I, to be issued shortly, has shown that the amount of carbon in solution within deformation bands varies considerably from point to point, depending on the proximity of a lenticular carbide. Where lenticular carbides are close, little carbon is in solid solution and it can be assumed it has left the deformation band and precipitated onto the lenticular carbides. On tempering, these areas show little or no carbide precipitation. Where no lenticular carbide has formed however, the carbon remains in solution within the deformation band and, on tempering in the microscope, this entrapped carbon is observed being released from solid solution to form many carbide precipitates within the deformation band.

Results of this tempering experiment are summarized by the two electron transmission micrographs of Enclosure 3. Both micrographs are of cell structures seen in the same specimen after it was tempered in the microscope. The upper micrograph shows no evidence of carbide precipitation after tempering at 550°C (2.5 hours) while the lower micrograph shows that many small carbide particles have precipitated during tempering at 325°C (2.5 hours).

The absence of carbide precipitation within a cell area indicates that the dissolved carbon level is low. This condition is found in cases where the cell structure is bounded by a lenticular carbide. Conversely, the presence of precipitated carbides indicates a high level of dissolved carbon. This condition was seen to exist only where no lenticular carbide is associated with the cell area. It is concluded therefore that the lenticular carbide serves as a "sink" which absorbs the excess dissolved carbon which, otherwise, would remain in solid solution within the cell structure.

Since carbon migration is necessary for the growth of lenticular carbides their formation and size will be time dependent. This is demonstrated in Enclosure 4 where sections from two bearings that are identical in all respects except for cycling times are compared.

The upper photo is from a bearing with 157 million revolutions (at 9700 rpm this is 270 hours of operation) while the bearing section shown in the lower photo experienced 383 million revolutions (660 hours). Both bearings are from the same homogeneous test group. It is apparent that lenticular carbides in the lower photograph are considerably thicker than those in the specimen with shorter running time.

In the case of deformation bands produced in a very short time; for example, in a single cycle of load application, there should be no evidence of lenticular carbide formation. This is shown in Enclosure 5 which is a section made through a hardened bearing ball that was crushed in a press. Extensive areas of white etching, plastically deformed material can be seen in the vicinity of the cracks. There are no lenticular carbides and there is little, if any, evidence of carbide dissolution.

The presence of lenticular carbides can therefore be taken as a measure of the time required to produce the adjacent areas of plastic deformation. Thus a distinction can be made between rapidly formed and slowly formed deformation bands. This distinction can be of value when assessing the stress raising potential of a defect or inclusion. Where rapidly formed white areas are seen around a defect it can be concluded that the defect was an effective stress concentrator. Such a defect is shown in Enclosure 6 where rapidly formed deformation bands can be seen around the inclusion.

Just as the large lenticular carbides are visible evidence of diffusion related alterations, the "white areas" are evidence of microplastic disturbances. Although not evident in the light microscope, this becomes clear when comparison is made between transmission electron micrographs made through a normal martensitic region and a white area. Enclosure 7 shows the marked change that takes place in a bearing steel during cyclic stressing. The transmission micrograph to the left, taken from an unstressed region shows the normal high carbon martensite structure as it appears after tempering at 240°C for 4 hours. The micrograph on the right taken within a white area shows a completely altered cell like structure.

In the altered structure, internal twins are no longer evident and the platelet appearance of the martensitic structure has been totally obliterated. As shown in the literature, the cell walls are formed from tangles of dislocations and it is clear that a great deal of dislocation motion had to take place to transform the previously existing, internally twinned martensite plate structure to a cell structure. In the process of forming a cell structure the small carbides which were precipitated during tempering have dissolved. The excess carbon so formed then travels to the borders of the cell area where it reprecipitates at convenient locations to form large lenticular carbides. A more detailed description of the formation of cell structures is given in (2).

In summary therefore, two types of micro-structural alteration are seen developing in hardened bearing steels during cyclic stressing. Plastically disturbed zones are seen under the light microscope as white etching areas while diffusion related changes are seen as lenticular carbides, usually surrounding the "white areas". The "white areas" have been designated as deformation bands since they are the product of plastic deformation and they are usually visualized on cutting planes where they appear as bands. In their true 3 dimensional form, however, they more closely approximate an irregular plate like shape.

The above discussion is limited to metallurgical changes in the structure and no mention has been made of crack formation or propagation. Cracking has been observed and is discussed later.

2) Geometrical Description of Deformation Bands

The shape of deformation bands and their orientation to the contact surface has been determined by viewing them on various cutting planes made through laboratory endurance tested 6309 size bearing inner ring specimens of common bearing steels (52100 M50, 52CB and several specimens of ausformed M50 steel). Enclosure 8 shows schematically the principal cutting planes that were examined.

On axial sections, deformation bands appear as shown in Enclosure 1 and are oriented parallel to the contact surface. Typically, their length to width ratio is of the order of 25:1 and it is not unusual to encounter bands as long as 0.015" (0.3mm) in specimens where they are well developed. In the axial view, elongated, sharply bounded structures can be seen associated with, and generally bordering, the white etching deformation bands. It was shown by a series of tempering experiments described in (3), that these elongated structures are carbides.

On circumferential cutting planes, the deformation bands again appear as structures that are long with respect to their width. On these planes, however, they are no longer parallel to the surface but are oriented at a definite angle to the contact surface as shown in Enclosure 9. The angular orientation seen in the 6309 deep groove bearing configuration is invariably close to 23°, rising toward the surface in the direction of ball travel. Cylindrical bearing inner rings have been examined and the angle found was close to 30°. Apparently the angle formed is functionally related to the bearing geometry in a manner that is not presently understood.

Views on the axial and circumferential planes suggest that the deformation bands are actually thin platelets oriented to the surface at a 23° angle (in 6309 inner rings). As shown in Enclosure 10 where the deformation bands are viewed in their own plane (i.e. a plane cut 23° to the ring tangent) they have an irregular plate like appearance.

3) Location of Deformation Bands and Their Relationship to the Calculated Stress Level

It was shown in (3) that the concentration of deformation bands varies with depth in a manner that is analogous to the variation of the maximum (unidirectional) shear stress (max) with depth. The maximum density of deformation bands is found at a depth below the contact surface that corresponds closely to the depth where max. reaches its highest magnitude. Most specimens

of the 6309 configuration examined to date (with some notable exceptions to be discussed later) have shown a well defined upper limit to the deformation bands, located at a depth between 0.008" to 0.009" below the contact surface. This finding as well as the general correspondence between the density of deformation bands and the maximum shear stress curve, mentioned above, suggest that deformation bands develop only when a critical shear stress magnitude is exceeded.

It was shown in (2) that this critical value can be estimated at max.=120,000 psi. This estimate is based on the observed limits of deformation bands seen on axial planes cut through the 6309 inner ring configuration. Enclosure 11 gives details of the contact and shear stresses generated during operation of this configuration under the standard test loading conditions employed. Enclosure 12 is a low magnification micrograph showing the distribution of deformation bands on an axial plane with a superimposed plot, drawn to the same scale, showing calculated contour lines which connect points that have experienced equal magnitudes of max. shear stress. It is impossible to draw a single contour line which includes all of the deformation bands without extending it well into the region where no deformation bands exist. The actual distribution of deformation bands appears to be deeper and concentrated more towards the center than predicted by the calculated shear stress values. It is believed nevertheless that 120,000 psi is a realistic estimate of the threshold shear stress since it most closely approximates the observed limits of deformation banding.

This estimate is limited to 52100 steel, heat treated to a hardness of Rc 59-60 with no retained austenite. Similar estimates made on other materials or on different 52100 steel structures may be valuable indicators of the response of materials to cyclic stress.

4) Rate of Deformation Band Development

It seems intuitively reasonable that, if deformation band development is related to cyclic stress, their concentration should increase with longer cycling times. In general, this was found in (2) to be true for specimens selected from the same test group although there are unexplained deviations from this behavior and there is quite a large scatter in a plot of % structural alteration vs. cycling time. A large difference was found (2) also between the rate of structural change in a group of non-stabilized bearings (15% retained austenite) and two groups of stabilized bearings (0% austenite austenite). The group with retained austenite developed deformation bands at approximately 2 to 3 times the rate of the stabilized groups.

This difference is ascribed to the fact that retained austenite is a softer consituent than martensite or the lower bainite structures formed during decomposition of retained austenite. Thus retained austenite, having a lower yield point, deforms plastically more readily in response to the cyclic shear stresses generated during rolling contact.

It would be tempting at this point to postulate either a beneficial or a harmful effect on fatigue life, from high rates of deformation band growth. In the study reported in (2) the data seemed to indicate that higher L_{10} group lives are related to greater rates of deformation band growth. This result could not withstand a test of statistical significance, however, and is considered accidental particularly since some recent work, to be discussed later, has shown that excellent L_{10} lives are associated with bearing groups that developed no deformation bands.

PART II

IDENTIFICATION OF POTENTIAL FAILURE INITIATION POINTS

In the previous section, discussion has centered on the growth of deformation bands at predictable locations within the highly stressed volumes of bearing parts. The question arises whether deformation bands are relevant to the problem of fatigue failure or merely concurrent to cycling, i.e., a phenomenon which accompanies cycling but bears no relationship to the actual failure mechanism.

The most serious doubts pertaining to the relevancy of deformation bands to fatigue are raised when the following facts are considered:

1) Fatigue failures are frequently seen in relatively short lived bearings which, upon sectioning, show little or no development of deformation bands within their highly stressed volume.

2) Unfailed bearings can be found with a high density of deformation bands throughout their stressed volume.

It has been concluded nevertheless, on the basis of observations to be described in the present report, that deformation bands are in fact intimately related to the rolling contact fatigue failure process. The apparent paradox disappears when a distinction is drawn between bulk material deformation bands and those that develop locally around imperfections.

Bulk material deformation bands are those that develop in response to the applied macroscopic stress field. They are typified by those shown in Enclosure 12 where the deformation bands have developed within a reasonably well defined area that has experienced repeated applications of a maximum shear stress in excess of an apparent threshold value; 120,000 psi (calculated). Localized deformation bands, on the other hand, arise at unexpected locations where the calculated shear stress may or may not exceed the apparent threshold value. Invariably, this type of deformation band is found associated with an imperfection. Localized deformation bands have, to the present time, been seen developing in the vicinity of 4 types of defects:

1) Non-metallic inclusions

2) Surface grinding furrows

3) Debris dents of the surface

4) Pits in the surface

Undoubtedly, there exists a number of other types of imperfections that can initiate the development of localized deformation bands. Any type of large dent, gouge, or pit resulting for example, from mishandling, passage of electric current, or corrosion would probably initiate local deformation band growth. These, however, are obvious failure causes and research efforts associating them with failure would be redundant. The defects listed above, however, are small, barely visible, imperfections that are usually seen only on examination under a low power microscope. Furthermore, they are imperfections that must be considered as normal occurrences, they are not the consequence of any unusual manufacturing or operating conditions.

In the following sections each of these imperfections will be discussed. A series of photographs will be presented showing the localized development of the deformation bands around imperfections. The sequence of events which eventually leads to spalling failure of the bearing part will be demonstrated.

1) Non-Metallic Inclusions

There is little need for further documentation of failures developing from large non-metallic inclusions in bearing parts. They are well known failure initiators and many examples can be found in the literature (12) showing their involvement in fatigue failures. Enclosure 13 is an example from the present study of an incipient spall that initiated at a large non-metallic inclusion.

What is lacking in the literature, however, is sufficient information concerning the effects of small inclusions in rolling contact fatigue of hardened steel.

There is some evidence in the literature taken from non-rolling contact fatigue investigations, showing that even very small inclusions can be effective failure nuclei. Cummings, Stulen and Schulte (13) did an extensive investigation of the inclusions which nucleated fatigue failure in a large series of rotating bending fatigue test specimens. They found that inclusions as small as 250 microinches (approximately 6μ) are effective initiators of fatigue failures in steel hardened to an ultimate tensile strength of 300,000 psi (approximately 53-55Rc). Duckworth (14) has summarized a number of fatigue investigations and makes the following statement regarding inclusions, "Where the inclusion is close to the surface it is clear that to achieve a fatigue limit of 200,000 psi would require inclusions no greater than 1μ in diameter to be present".

It is not the purpose of the present discussion to fix the critical size of harmful inclusions in bearing steels. This value is undoubtedly a function of the stress level, hardness level and quite possibly other properties of the bearing material such as ductility. It is being pointed out, however, that very small inclusions near the limit of light microscope resolution, are potential sources of fatigue failures. Enclosure 6 shows an incipient spall forming around a non-metallic incluions lying near the surface having approximately 10-15μ in diameter. Enclosure 14 shows very small sub-surface inclusions (less than 5μ) with deformation bands beginning to form in their vicinity.

2) Surface Furrows

The initiation and formation of spalls around surface furrows can best be demonstrated by a sequence of photos showing progressive stages of spall development.

Enclosure 15 is a surface photograph of an endurance tested bearing showing the typical effects that are associated with grinding furrows. The area surrounding the furrow is glazed and appears pulled or pitted in places within the glazed area. The visibility of glazing has been greatly enhanced by the fact that the bearing ring was lightly etched before running. This explains why the undisturbed surface away from the furrow appears dark.

After polishing the surface metallurgically with diamond paste (since the surface is curved, polishing is done manually with a small cotton swab) it is possible to see that the pitted region around the furrow is in fact a series of small cracks. This can be seen in Enclosure 16 where the polished surface adjacent to the furrow is shown unetched and, at somewhat higher magnification, etched. After polishing approximately 3 to 5μ below the surface, deformation bands lying below the glazed area of the surface are exposed. This is shown in Enclosure 17 where the deformation bands tend to form two parallel rows which lie in an approximate chevron formation when viewed on a polished surface parallel to the original surface.

Enclosure 18 shows incipient spalling under a furrow that was polished away to reveal the deformation bands. The beginning of a spall can be seen in its relationship to the deformation bands. The fact that the incipient spall fits neatly within the parallel rows of deformation bands is good evidence that cracks associated with the deformation bands are capable of joining together to form a small spall. The small spall eventually becomes a large spall which ends the useful life of the bearing. A typical furrow initiated large spall which caused failure at 150 million revolutions is shown at the top of Enclosure 19. At the bottom of the Enclosure is a cross-section cut through the spall as shown in the schematic diagram. Heavy deformation bands can be seen lying below the grinding furrow and leading directly into the spall.

The sequence of events leading to fatigue failures that initiate at grinding furrows can be summarized as follows:

The elastohydrodynamic oil film, which under the test conditions normally keeps the bearing surfaces separated in the contact area, collapses in the vicinity of the grinding furrow due to oil leakage into the furrow. This allows metal to metal contact to occur at the borders of the furrow, leading to the glazed appearance of Enclosure 15. Heavy tractive forces which greatly intensify the local stress field are presumably generated when the metal surfaces come into contact. The increased stresses cause localized plastic disturbances which in turn leads to cracking as shown in Enclosure 16. The cracks eventually join to form an incipient spall (Enclosure 18) which then grows to become a full scale spall that ends the useful life of the bearing (Enclosure 19).

3) Debris Dents

Essentially the same sequence of events which lead to furrow initiated fatigue failures can be seen operating in the vicinity of debris dents. Debris dents can form during test operation even though the oil supplied to test bearings is first passed through a 25μ filter. It is not unusual to find debris dents larger than 25μ in diameter on long lived bearings even though none of the bearing components have visibly failed during testing.

Enclosure 20 is a surface micrograph showing a debris dent with an incipient spall immediately above the dent. In the top micrograph the dent appears as a shallow depression while the incipient spall is the much deeper depression above the dent. Considerable glazing around the debris dent is apparent while a somewhat lesser degree of glazing can be seen around the incipient spall.

The spall outlined in the upper micrograph is shown in the lower micrograph at higher magnification after polishing (by rubbing with diamond paste on a cotton swab), and etching. After polishing, the outline of the dent is lost and it has been sketched in to show the relationship between the dent and the spall. By referring to the sketched outline it can be seen that the deformation bands have developed under the glazed areas surrounding the spall and not under the dent itself. It is also apparent from the relative positions of the spall, the dent, and the deformation bands that the most severe damage occurs under the glazed area rather than under the dent. This is consistent with the findings around grinding furrows. The parallel arrays of deformation bands seen on the polished surface of Enclosure 17 correspond to the glazed area around the furrow and relatively little plastic deformation is seen under the furrow itself. The final stages of spalling from debris dents (i.e. full scale spalls which constitute bearing failures) will be shown later in a discussion of spall analysis.

4) Pits

Recent observations have revealed that still another type of surface defect is associated with fatigue failures. These are presently being classified as pits to differentiate them from debris dents. Although at times it is difficult to differentiate between the two, pits generally are deeper and their bottoms tend to be darker, as though they had been subjected to chemical attack. The origin of the observed pits is unknown although a program, to be discussed later, has been initiated in an attempt to determine their origin.

Enclosure 21 includes two micrographs of fatigue damage around a pit. The upper photo shows a typical pit with the surrounding glazed and cracked area (compare with the dent in Enclosure 20 and note the greater depth and the dark appearance of the bottom). The lower photo taken after polishing and etching shows a number of cracks around the pit.

Clearly the type of damage around pits is identical to that previously shown around grinding furrows and debris dents. Here again the most severe damage is under the glazed area rather than under the defect itself. Examples of full scale spalls initiated at pits will be shown later.

PART III

SPALL ANALYSIS

In the traditional view of rolling contact fatigue it has long been held that failures are generally subsurface initiated (15). In the preceeding section it was shown that at least 3 types of defects can initiate failures at the surface. A number of surface originated failures have been documented in well made bearings. Thus it has now become possible to identify and to a degree control these additional sources of fatigue failure. These findings are of considerable practical significance.

1) Spalls Developed from Intentionally Produced Defects

One of the points emphasized in the proceeding section is that the most severe damage associated with a surface defect is found under the glazed area surrounding the defect. In examining failed bearings, it is frequently seen that the defect remains intact with the spalled area lying directly behind it in the direction of rolling. This was verified by intentionally producing defects on several bearing rings and examining them after failure. Enclosure 22 shows a bearing that was tested with a scratch produced with a pyramid shaped diamond and running across the groove in a direction perpendicular to that of ball travel. The scratch is shown before running at the upper left of Enclosure 22. A Talysurf trace is shown to the upper right and indicates that the scratch is approximately 0.0004" deep. The photograph at the bottom shows the same scratch after the bearing failed.

It is apparent that the scratch is intact and that failure started under the glazed area immediately adjacent to the scratch.

Enclosure 23 shows two examples of spalls that were initiated adjacent to grinding marks that were made with a hand grinder to simulate severe dents. Again, failure can be seen initiating under the glazed area with the grinding marks remaining intact on the surface. These examples are shown to illustrate the fact that it is not unusual to find the failure initiation point remaining intact on the bearing surface after a spall has developed. With respect to ball movement, the initiation points have always been found lying ahead of the spall, i.e. the ball rolls over the initiation point first. It is reasonable, however, to suspect that in many other cases this is not true, i.e. that the spall propagates both ways from, or directly under the initiation point. In these cases, evidence of surface initiation would be removed with the spall and the spall would be classified as indeterminate in origin.

2) Fatigue Spalls with Determined Point of Origin

A large number of spalls have been photographed in order to demonstrate the various types of spalls that have been identified in test ball bearings. It is emphasized that these photos do not include many types of failures that can be experienced in field operated bearings (See for example ref. 20). The test bearing photographs are not intended to demonstrate all of the bearing failure modes (i.e. lubrication distress, overloading, etc.) but rather to illustrate that there are various sub-categories of spalling failures that can be identified among that type of failure categorized under the general heading of fatigue failures.

The three types of surface initiated spalls are illustrated in the following enclosures:

Enclosure 24-Furrow initiated spalls.
Enclosure 25-Debris dent initiated spalls.
Enclosure 26-Pit initiated spalls.

Furrow initiated spalls are easily identified by their pointed ends (shown circled in Enclosure 24) which typically trail off into the furrow itself. Under binocular microscope examination (8-30X) the end of the spall near the furrow has a shallow slope while the other end typically has a steep slope. Reasons for this spall morphology will be examined later. The surface adjacent to the spall is always glazed and in some cases shows evidence of cracking similar to that shown in Enclosure 15. Glazing, in the spall photographs appears as a darkened region around the surface defect. This, in the low magnification photographs is due to oblique lighting conditions under which the pictures are taken. The high magnification photographs shown earlier (Enclosures 15, 20, 21) were taken on a Bausch and Lomb metallograph where lighting is perpendicular and glazing appears in its commonly seen contrast, i.e. the glazed area is lighter than the surrounding unglazed regions.

The debris dent initiated spalls of Enclosure 25 were chosen from bearings with no history of failure among the other rolling elements. As was pointed out earlier, origin of the debris which caused denting is unknown since it did not originate from visible failure of another element within the bearing.

A potential source of debris which could conceivably have caused the denting is material removed from the spall itself. This explanation cannot be justified, however, in view of the high degree of glazing observed around the initiation point which is greater than around the spall edges. Glazing takes time to develop and its severity testifies to the fact that the dent existed before the appearance of a spall. Upon spalling, the bearing begins to vibrate excessively and the test is shut down automatically by a vibration sensing device within minutes after spalling first occurs. Experience with test bearing operations has shown that glazing will develop around small surface marks, such as the dents shown, only after prolonged bearing operation.

Further evidence that dents preceed and in fact cause spalling was given earlier where the development of deformation bands and an incipient spall adjacent to a dent was shown (Enclosure 20). Finally, there is evidence from spall morphology where, as shown previously with furrows, the shallow end of the spall lies immediately adjacent to the dent point of initiation.

Enclosure 26 shows pit initiated spalls. The origin of this type of surface defect has not been determined. The bottom of the pits frequently appear darkened as if there were corrosive attack on the meta. No known cause exists, however, for corrosion in the test environment. The pits are not restricted to the region of the spall and they are seen on both failed and unfailed bearing elements. In cases where spalling appears to be pit initiated, numerous other pits are generally found on unfailed portions of the contact surface. Few, if any, are seen on non-contact surfaces. The detection of pitting, which appears to be corrosion related, in a presumably non-corrosive test environment is a significant finding that will be pursued in future investigations.

Under binocular microscope examination dent and pit initiated spalls are frequently difficult to distinguish from each other and in photographs the difference is even harder to detect. In cases where the spall is clearly dent initiated, the dent has a definite outline with a clean appearing bottom that appears as a depressed region showing the same markings as the surrounding surface. Initiation points that are clearly pits however are irregular in outline and show the discoloration at the bottom mentioned previously. There are a number of surface defects which have some characteristics of both and the decision whether they are classified as dents or pits rests largely with the observer.

This situation, as well as the fact that both dents and pits are of unknown origin shows the need for further investigation that will determine at what point in running these features develop and when their effects becomes serious enough to initiate failures. It is planned, in this program, to study the changes in surface condition that develop during bearing operation by taking photomicrographic records of bearing surfaces at periodic intervals in the course of endurance testing. Evidence that pits have the same capability of initiating fatigue failures as do dents and furrows was shown earlier in Enclosure 21. Pit initiated spalls show the same morphology as do the other two types of surface initiated spalls, i.e., the side of the spall next to the pit has a shallow entry slope while the opposite end of the spall has a steep slope

3) Fatigue Spalls of Indeterminate Origin

In paragraph 2, above, three types of fatigue spalls with identifiable origins were described. Not all test bearing failures fall into these categories and there remains a number of failures where the point of initiation cannot be readily identified. These failures of indeterminate origin have distinctive appearances which make it possible to classify them into two categories shown in Enclosure 27 and described as follows:

A) Apparently Surface Initiated Spalls with no Obvious Point of Initiation

These spalls have much the same morphology as do the other surface initiated spalls, however, no dent, pit or furrow appears at the shallow spall end. It is conjectured that this type of spall originates either at an inclusion that lies near the surface or at a surface defect that was removed during spalling.

B) Apparently Subsurface Initiated Spalls

It is shown later that a high percentage of spalls among endurance tested bearings originate at surface defects. There remains however a sizable number of spalls with no identifiable initiation point and no evidence of surface initiation. This type of spall shown at the bottom of Enclosure 27 is the only category which shows no shallow end and at least some of these spalls are believed to initiate at subsurface inclusions.

It should be emphasized that the findings of the present report, with regard to surface initiated spalls, have generally been made on endurance test bearings produced from exceptionally clean heats of through hardening steels that have been prepared by consumable vacuum remelting (CVM) or carbon vacuum deoxidation (CVD) processes. These are among the cleanest bearing steels available. The bearings are generally operated in a test regime where adequate elastohydrodynamic (EHD) conditions prevail (EHD film thickness to surface roughness ratio greater than 4).

The proportion of subsurface originated failures will, for a given EHD film condition, tend to increase with increasing inclusion content. With lower EHD film thickness/surface roughness ratios however the trend will be towards increased surface originated failures.

Although the data presented has emphasized the surface initiation of spalls it is not intended to de-emphasize the importance of subsurface initiation at large non-metallic inclusions. Among those steels with relatively abundant or large non-metallic inclusions (e.g. air melt, through hardening steels and non-vacuum melted carburizing grades of steel), subsurface initiation remains an important mode of spalling. Even among the bearings made from clean steels, described later in this section, a significant number of spalls are of undetermined origin. These spalls are suspected of being subsurface initiated.

Investigations of the failure nuclei in spalls with undetermined regions are currently being made by electron microscope examination of spall fractographs, a technique recently developed at the SKF Laboratory.

4) Spall Fractography

The electron microscope offers a distinct advantage over the light microscope for spall investigations in that it is capable of resolving details at high magnification while maintaining a large depth of focus. At equivalent magnification the light microscope image of a rough surface is largely out of focus and only a very limited area is visible. Furthermore, the upper limit of available magnifications is greatly extended.

The technique developed for examining spalled bearing surfaces involves making a two stage, polystyrene carbon replica. The technique is fully described in a Special Report to be issued shortly (AL67M060).

Electron microscope studies of fracture have shown a variety of fracture modes which can be classified into the two broad categories of ductile and brittle modes. Between these extremes are certain types of fracture surfaces which bear some aspects of both modes.

It is hoped in these spall fractographic studies, to determine what portion of spall formation is by slow crack propagation (generally associated with ductile fracture modes) and by catastrophic crack growth (brittle fracture).

Although only a limited number of spalls have been examined to date, the available evidence supports the contention that cracks leading to spalls in through hardened bearing rings propagate predominantly by brittle fracture modes. Enclosure 28 is a typical example of the "cleavage" type of fracture surface which seems to predominate over the major portion of spall surfaces. (Pelloux (16) has summarized a number of microfractographic investigations and considers cleavage as a brittle mode of crack propagation).

A few isolated examples of ductile fracture modes have been found in spalls. Enclosure 29 shows a second phase particle (presumably a non-metallic inclusion) which appears to have initiated a series of step-like fatigue striations in the surrounding material.

This fractograph is from a spall that was believed to be subsurface initiated. Although it is not possible to show that the particle was responsible for failure of the ring, it is evident that fracture, within the region shown, initiated at the particle. A considerable body of data as well as experience in interpreting fractographic evidence must be gained before it will be possible to make conclusive identifications of failure initiation points.

5) Relative Frequency of Various Spall Types

Any tabulation showing the relative frequency of the various spall types will necessarily be influenced by a number of paraemters including; the material tested, operating conditions, e.g. speed, lubricants, etc.

It is interesting nevertheless to show such tabulations for several recent bearing test groups in order to demonstrate that surface initiated failures are not isolated occurrences and represent an important mode of fatigue failure. It is emphasized that these tabulations are representative of high cleanliness, through hardened bearing steel run under the carefully controlled laboratory test conditions specified in Table I.

TABLE I

Test Conditions for All Endurance Test Bearings Described in Described in Tables II, III, IV

Bearing Type	- 6309 Deep groove ball bearing
Load	- 4240 lbs. radial load (See Enclosure 11 for further details).
AFBMA Calculated L_{10}	- 10 million revolutions
Test Machine	- R-2
Speed	- 9700 rpm
Lubricant	- Mobil DTE extra heavy mineral oil, circulating
Outer Ring Temper.	- 95-105 degrees C

TABLE II

Spall Types Identified in a Group of Consumable Vacuum Remelted 52100 Bearings

Surface finish-ground & polished,11 microinches AA

Elastohydrodynamic film thickness/surface roughness ratio (calculated)=2.0

L_{10} life estimate*-50.8 million revs.

26 Brgs. tested-22 inner rings failed*-20 inner rings examined

Ring Life	Spall Type	Ring Life	Spall Type
14.3 million	Indeterminate	170.1 mill.	Furrow initiated
24.6 million	Furrow initiated	179.3 mill.	Furrow initiated
26.3 million	Furrow initiated	198.8 mill.	Furrow initiated
50.3 million	Furrow initiated	240.5 mill.	Furrow initiated
53.4 million	Indeterminate	245.2 mill.	Furrow initiated
71.9 million	Furrow initiated	264.2 mill.	Furrow initiated
74.3 million	Furrow initiated	309.8 mill.	Indeterminate
128.6 million	Furrow initiated	339.8 mill.	Furrow initiated
141.7 million	Furrow initiated	344.6 mill.	Undeterminate
148.8 million	Furrow initiated	392.4 mill.	Undeterminate

(Bearing identification-F1042 Group 2.1)

*It is customary in bearing endurance tests for the inner ring to be the test element since this is the critical part most likely to fail. In cases of outer ring or ball failures, they are considered as suspensions. L_{10} is estimated by bias corrected maximum likelihood method. For this reason all life results and spall analyses are for inner rings only.

This bearing group was tested in 1960 when grinding and polishing was the standard surface finishing technique for these test bearings. It is apparent that furrows were the predominate cause of failure in this group with a surface finish of 11 microinches (arithmetic average). Since that time the final polishing operation has been replaced by honing which produces superior surfaces as shown below.

TABLE III

Spall Types Identified in a Group of Carbon Vacuum Deoxidized 52100 Steel Bearings

Surface Finish-Ground and Honed 1.3-2.0 Microinches

Elastohydrodynamic film thickness/surface roughness ratio (calculated) = 9.4

L_{10} Estimate - 95.0 million

29 bearings tested-13 inner rings failed

Ring Life	Spall Type	Ring Life	Spall Type
69.1	Furrow initiated	223.1	Indeterminate
87.3	Pit initiated	224.5	Furrow initiated
141.1	Indeterminate	256.7	Indeterminate
153.2	Furrow Initiated	314.3	Indeterminate
155.6	Indeterminate	349.6	Furrow initiated
156.7	Furrow initiated	377.3	Indeterminate
191.6	Furrow initiated		

Bearing identification F-6891

In this group, with improved surface finish, the proportion of furrow initiated failures decreased while the bearing lives increased.

The following three bearing groups were manufactured from experimental heats that are molybdenum containing modifications of 52100 steel (one steel analysis is known as 52CB). These groups gave excellent L_{10} lives.

TABLE IV

Spall Types Identified in Three Groups of Experimental Modifications of the 52CB Steel Analysis

Group 1-Acid openhearth airmelt 52CB modification

Surface Finish-1.3-2.5 microinches-ground & honed

Elastohydrodynamic film thickness/surface roughness ratio (calculated)=8.2

30 bearings tested-4 inner rings failed

L_{10} life estimate-329 million revs.

Ring Life	Spall Type	Ring Life	Spall Type
213.1	Indeterminate	350.6	Indeterminate
279.7	Dent initiated	401.2	Dent initiated

TABLE IV (Cont'd)

Group 2 - Consumable vacuum melt 52Cb modification

Surface finish-1.6-2.4 microinches-ground & honed

Elastohydrodynamic film thickness/surface roughness ratio (calculated)=8.0

32 bearings tested-5 inner rings failed

L_{10} life estimate - 176 million revs.

Ring Life	Spall Type	Ring Life	Spall Type
36.0	Dent initiated	249.0	Furrow initiated
50.5	Indeterminate	311.0	Dent initiated
185.5	Indeterminate		

Group 3-Acid openhearth air-melt 52CB modifications

Surface finish-1.3-2.2 microinches, ground & honed

Elastohydrodynamic film thickness/surface roughness ratio (calculated)=8.6

32 Bearings tested-3 failed

L_{10} life estimate-414 million

Ring Life	Spall Type
321.7	Furrow initiated
335.8	Pit initiated
420.1	Indeterminate

Even though these last 3 groups have excellent lives, surface originated failures played an important role in determining the group lives.

Examination of unfailed bearings from these modified 52CB steel groups showed that many long lived rings (300-500 million revs.) had dents and pits that did not cause failure. Several long lived bearings (300-500 million revs.) from each group were sectioned and examined under the light microscope for evidence of deformation bands. Repeated thorough examinations were made on axial cross-sections within the bulk material zone where the deformation bands are normally found. No evidence of bulk material deformation bands were found in any of these specimens. This is in direct contrast to the usual experience with other materials (including the basic 52CB analysis) where copious deformation bands can usually be found in the highly stressed portions of the rings after 100-200 million revs. at the same test load. A number of dents and pits on the ring surfaces were polished and again no evidence of deformation bands were found.

The absence of deformation bands in either the subsurface bulk material or around surface defects, coupled with the long life demonstrated by this material is taken as evidence that in this steel the threshold shear stress for initiation of deformation band growth probably exceeds the value estimated for 52100 steel (120,000 psi). Thus, the modified 52CB material appears to be more resistant to plastic deformation under stress cycling and should therefore be more fatigue resistant.

6) Ultrasonic Detection of Incipient Spalls

A disadvantage of the spall analysis methods, described above, for detecting failure nuclei lies in the fact that once spalling has taken place there is a distinct possibility that the nucleation point has been obliterated by continued catastrophic cracking and spalling.

Existing endurance test equipment has been modified as shown in Enclosure 30 for use with ultrasonic equipment which has been designed to monitor the stressed volume of a test piece throughout the entire rolling contact endurance test of a flat thrust washer/ roller configuration. Information from the test is recorded on a continuously running Alfax recorder.

As originally conceived the test was designed to operate as follows:

If a defect is seen by the ultrasonic beam within the stressed volume, this will be recorded as a dark point on the recorder scan line. The horizontal position of the defect on the recorder scan line can be related to its azimuth position within the specimen by noting its distance from the origin of the scan line, as shown in Enclosure 31. Thus as each succeeding scan is recorded directly below the previous scan line, the same defects will be noted over and over. As the chart continues to feed out at a rate of 10 inches per hour, the repetition of defect indications at the same horizontal positions will become visible as vertical lines. Since random noise indications are not repeated at the same azimuth locations they will not line up vertically and it should be possible to detect true defect indications even if weaker than random noise pulses. As cracks are initiated and begin to grow, either new indications will become visible or the existing indications will begin to become more prominent.

The test washer being monitored developed a small spall (approximately 1/16" X 1/16") on the inner edge of the rolling path after running a total of 380 hours. No unusual ultrasonic indications were recorded either before or after the spall was noted. Previously the ultrasonic equipment had been checked and found capable of detecting Rockwell hardness indentations located at the center of the ball path (this was done on a different non-test washer).

With the test machine shut down it was possible to detect the spall ultrasonically by repositioning the ultrasonic test head. Failure to detect the spall during running is therefore ascribed to the fact that the ultrasonic beam was focussed primarily at the center of the rolling track. The track is 5mm wide and apparently the beam is incapable of detecting defects over the entire path width in spite of the fact that the ultrasonic crystal was designed to do so.

The ultrasonic test is being re-evaluated and a decision will be made in the near future to either redesign the ultrasonic search and recording system or to discontinue the test.

PART IV

Crack Propagation Along Deformation Bands

The preceeding section has dealt almost exclusively with crack initiation with little mention being made of crack propagation. In Progress Report III (5) the directions of crack propagation in the vicinity of spalls were documented by a large number of photographs showing repeated cross-sections made through spalls. This study led to the conclusion that cracks propagate at an acute angle towards the bore of the ring until they meet deformation bands whereupon they are diverted back towards the surface in the direction of ball travel. This is shown schematically in Enclosure 32.

A striking example of this spall formation in an actual bearing is shown in Enclosure 33. At the top of the Enclosure is a photo of the spall before sectioning. Evidence of a furrow initiation point can be seen at the left side of the spall while the spall bottom has a distinctive serrated appearance. The line drawn through the spall shows the sectioning plane which was cut parallel to the direction of ball movement. Micrographs of the cross-section are shown pieced together at the bottom of Enclosure 33. The portion shown in Enclosure 33 represents only a small segment of the sectioning plane under the furrow. The "sawtooth" surface shown was taken from a two foot long display of pieced together photographs which, in its entirety is too cumbersome to show here. It is apparent that the cracks propagate along deformation bands and that the portion of the spall surface which slopes upward (in the rolling direction) towards the original contact surface, tends to follow along the surfaces of deformation bands.

Referring back to the spall photograph at the top of the Enclosure it is now apparent that a portion of the serrated surfaces that are oriented to reflect light (the shiny surfaces) are actually deformation bands that have become exposed by removal of the surface material through spalling. Some of the deformation bands of course are removed when the mating pieces of the spalled material are torn away.

Additional evidence of crack propagation along deformation bands was shown in the First Summary Report (1). When endurance tested rings containing deformation bands were fractured in a press, the fracture paths deviated markedly from their original courses in order to propagate along deformation bands. Once past the region of deformation bands, the fracture paths resumed their original course.

It is conjectured that lenticular carbides which form preferentially at the boundaries of deformation bands, are responsible for this behavior. The lenticular carbide boundaries are believed to be brittle interfaces which represent preferred paths for crack propagation.

When the spall initiates at a surface defect, the end of the spall near the defect has a shallow slope. In Enclosure 19 the localized near-surface deformation bands, associated with the defect at the shallow end of the spall, are oriented in a direction that is opposite to that shown in Enclosure 9 for the subsurface bulk material deformation bands. With respect to the rolling direction, the near surface deformation bands slope downwards away from the surface while the subsurface bulk-material deformation bands slope upwards towards the contact surface.

In Enclosure 19 it can be seen that the spall surface, at its shallow end, slopes in the direction of the near surface deformation bands. It is believed that cracks propagate in this direction to a depth sufficient to bring them in the vicinity of the subsurface deformation bands. In the subsurface region the direction of crack propagation is altered by the bulk material deformation bands which tend to divert the cracks back towards the surface.

This behavior is demonstrated in Enclosure **33** by a specimen with well developed bulk material deformation bands. The same behavior has been demonstrated in Progress Report III (5) in a specimen with very few bulk material deformation bands. It was also shown in (1) by a series of spall depth measurements, that the maximum depths attained by spalls corresponds to the depths where bulk material deformation bands are found.

PART V

DISCUSSION AND APPLICATION OF RESULTS

Discussion

Deformation bands have been shown to be relevant to rolling contact fatigue in two respects:

1) They are preferred paths for easy propagation of cracks.

2) Their location and density is an indication of the stress level achieved during cyclic stressing. In this sense they are a type of "strain gage".

When observed in the bulk material, deformation bands are an indication of the macroscopic stress level imposed during bearing operation. In cases where bearings with unknown or suspect loading conditions are examined, the location and density of deformation bands can be compared with the calculated stress levels and inferences made with respect to the true loading conditions. For example, evidence of misalignment has been detected in cylindrical roller bearings by comparing the density of deformation bands at either end of the contact zone, with the greater concentration being found at the heavily loaded end.

Deformation bands have also been observed at locations where the calculated stress is well below the "threshold level" for their growth. In these cases they are invariably found to be associated with defects. Deformation bands around large non-metallic inclusions (e.g. "butterfly" structures) are well known examples of their localized growth around defects. In the present investigation, localized deformation band growth has been associated with several types of surface defects as well as with very small inclusions. The data presented earlier, linking defects to deformation bands, cracks, and spalls, has shown that the development of deformation bands around a defect can be taken as evidence that the defect is a potential failure nucleus.

In spite of this evidence and the evidence showing that cracks propagate along deformation bands, no evidence has been uncovered showing fatigue cracks initiating at the deformation bands themselves.

These results are consistent with observations made by Grosskreutz (17) who has summarized a number of fatigue investigations dealing with micromechanisms. He has concluded that, while many types of structural alterations are associated with fatigue processes, it is wrong to assume that the changes are a type of "fatigue damage" which if prolonged, will of themselves eventually lead to crack initiation.

In his view, however, fatigue cracks can be initiated by the interaction of micromechanisms with a free surface. Where subsurface initiation of cracks has been reported, initiation is generally associated with defects such as voids or inclusions that can act as a free surface. Grosskreutz feels that conclusive evidence, linking micromechanisms to bona fide cases of subsurface crack initiation (in an intact matrix) is lacking. Once a crack is initiated, however, there is little doubt that microstructural changes play a major role in its propagation.

With the recent advent of vacuum processes the cleanliness of steels is continuously improving. With fewer and smaller subsurface non-metallic inclusions being available to initiate fatigue failures the role of surface defects becomes more important. This is shown by the data of Table II where the fatigue failures are predominantly of surface origin in a group of vacuum melted steel bearings with a surface finish of 11 microinches AA which by todays standards for endurance test bearings is not the best. Improvements in surface finishing can reduce the importance of surface failures (as in Table III).

OUTLOOK

Findings made in the investigation suggest several future studies or practical applications.

Control of Surface Originated Failures

It can be concluded, from the evidence presented earlier, that surface defects are not of themselves entirely responsible for the localized stress intensification that leads to the observed damage. In every case, the damage has been found under the glazed area where elastohydrodynamic lubricant film conditions are not maintained.

While it is desirable, of course, to operate with surfaces as free of defects as possible, a certain amount of surface damage is unavoidable. The furrows, dents or pits will be far less effective as failure nucleation points, however, if metal to metal contact at their borders is prevented or their influence on failure is otherwise minimized. This can be accomplished by lubrication schemes such as further increasing the lubricant film thickness, using better boundary lubricants, or solid surface films.

It should be cautioned that large increases in bearing life through the control of surface originated failures can only be expected with clean bearing materials. If severe subsurface initiation points are readily available, as in a dirty heat of steel, little is gained by eliminating the surface initiation points. Failure always depends on the outcome of a competition between failures initiating at the most severe surface or subsurface stress raiser.

Investigation of the Limiting Size of Harmful Defects

At the present time information is almost totally lacking regarding the limiting size of "harmful" defects. The situation with regard to surface defects can be attacked, simply by making large numbers of measurements of surface defects that cause failure. Conceivably, functional relationships between defect size, life, and bearing operation parameters could be derived from such a study. A start in this direction will be taken in an investigation, to be initiated shortly, where bearing surfaces will be examined and photographed at various stages of interrupted endurance tests.

Selection of Bearing Steel Candidates by Physical Property Measurements

The estimated value (120,000 psi) of the threshold shear stress for deformation band growth in 52100 steel implies that there is a yield point significantly below that usually associated with hardened steels. This "microyield" limit is a measureable physical property. Since plastic deformation is required for the initiation and propagation of fatigue cracks, it is reasonable to postulate a relationship between the microyield limit and fatigue behavior.

Ductility is another material property that can be expected to correlate with fatigue. Manson (18) as well as Coffin (19) have shown that ductility is a key determinant of fatigue behavior in the low cycle range of fatigue failures. There is no reason to suspect that this relationship does not held for high cycle fatigue applications of hardened steel. Duckworth (14) has stated; "The requirements for producing steels with a high fatigue limit appear to be a raising of the tensile strength to above 400,000 psi (Rc 60 and above) while retaining a high ductility and keeping the size of deleterious inclusions to below 10μ".

Among steels hardened to the levels used for rolling contact bearings it is generally assumed that ductility is low and little attention has been paid to this material property.

With constantly increasing demands being made of bearings, operating in unusual environments at high or low temperatures, new materials and optimum heat treating parameters are continually being evaluated.

Faced with this large array of potential bearing material candidates, the standard endurance test method of evaluating materials is frustratingly slow and costly. Screening tests based on fatigue related material properties would be of great help in eliminating obviously poor candidates and would provide a rational basis for selecting the more promising candidate materials if it could be shown that such tests correlate with fatigue. While such attempted correlations have been fruitless in the past, better approaches may well be found.

REFERENCES

1) Martin, J. A. Borgese, S. F , Eberhardt, A. D., Chiu, Y. P., "Structural Studies of Bearing Steel Undergoing Cyclic Stressing", First Summary Report, Office of Naval Research, U.S. Department of the Navy, Contract Nonr 4433 (00).

2) Martin, J. A. Borgese, S. F., Eberhardt, A.D., Berlinghof, W., "Structural Studies of Bearing Steel Undergoing Cyclic Stressing", Second Summary Report, Office of Naval Research, U. S. Department of the Navy, Contract Nonr 4433 (00).

3) Martin, J. A., Borgese, S.F., Lee, E. U., Eberhardt A.D., "Structural Studies of Bearing Steel Undergoing Cyclic Stressing, Progress Report No. 1", Office of Naval Research, U.S. Department of the Navy, Contract Nonr 4433 (00).

4) Martin, J. A., Borgese, S.F., Eberhardt, A.D., and Lee, E. U., "Structural Studies of Bearing Steel Undergoing Cyclic Stressing" Progress Report No. 2, Office of Naval Research, U.S. Department of the Navy, Contract Nonr 4433 (00).

5) Martin, J. A., Borgese, S.F., Eberhardt, A.D., "Structural Studies of Bearing Steel Undergoing Cyclic Stressing", Progress Report No. 3, Office of Naval Research, U.S. Department of the Navy, Contract Nonr 4433(00).

6) Martin, J. A., Borgese, S.F., Eberhardt, A.D.,"Microstructural Alterations of Rolling Bearing Steel Undergoing Cyclic Stressing", Journal of Basic Engineering, September 1966, Transaction of the ASME pp. 555-567.

7) Klesnil, M., Lukas, P., "Dislocation Arrangement in the Surface Layer of Iron Grains During Cyclic Loading", Journal of Iron and Steel Institute, October, 1965, pp. 1043-1048.

8) Shrier, A., Yamamoto, Hil, Weissmann, S., "Fatigue of Metals Crystals", Technical Report No. AFML-TR-65-86 April, 1965, Air Force Base, Ohio.

9) Lawley, A., Meakin, J. D., Snowden, K. U., "Direct Study of Dislocations in Metals by Transmission Electron Microscopy - Fatigue Deformation" Final Summary Report Contract AF 33 (657)-10360, Report ARL 65-11 January, 1965.

10) Forsyth, P. J. E., Stubbington, C. A., "The Mechanism of Fatigue Failure on Some Binary and Ternary Aluminum Alloys" Journal of the Institute of Metals, 1956-57, Vol.85 pg. 339.

11) Wood, W. A., "Recent Observations on Fatigue Failure in Metals", Symposium on Basic Mechanisms of Fatigue ASTM Special Technical Publication No. 237.

12) Littman, W.E., Widmer. R. L., "Propagation of Contact Fatigue From Surface and Subsurface Origins" Journal of Basic Engineering, September 1966 Transaction of the ASME pp. 624-636 .

13) Cummings, H. N., Stulen, F. B., Schulte, W.C., "Tentative Fatigue Strength Reduction Factors for Silicate Type Inclusions in High Strength Steels", Proceedings of the American Society for Testing Materials, Vol. 58, A58, pp. 505-514.

14) Duckworth, W. E., "The Achievement of High Fatigue Strength in Steel", Metallurgia, Feb. 1964, P. 53-55.

15) Lundberg, G., Palmgren A., "Dynamic Capacity of Rolling Bearings" Acta Polytechnica, Mechanical Engineering Series Vol. 1 No. 3.

16) Pelloux, R. M. N., "The Analysis of Fracture Surfaces by Electron Microscopy", ASM Metals Engineering Quarterly, November, 1965.

17) Grosskreutz, J. C., "A Critical Review of Micromechanism in Fatigue", Fatigue An Interdisciplinary Approach, Proceedings of the 10th Sagamore Army Materials Research Conference, Syracuse University Press, 1964.

18) Manson, S. S., Hirschberg, M. H., "Fatigue Behavior in Strain Cycling in the Low and Intermediate Cycle Range" Fatigue An Interdisciplinary Approach, Proceedings of the 10th Sagamore Army Materials Research Conference, Syracuse University Press, 1964.

19) Tavernelli, J. F., Coffin, L. F., "Experimental Support for Generalized Equation Predictin Low Cycle Fatigue", Transactions of the American Society of Mechanical Engineers, Vol. 84, Series D, No.4, December 1962, PP. 533-541.

20) Tallian, T. E., "On Competing Failure Mode in Rolling Contact", Presented at the 22nd ASLE Annual Meeting in Toronto May 1-4, 1967, Preprint No. 67AM1C-3, American Society of Lubrication Engineers.

AL67M050

ENCLOSURE 1

DEFORMATION BANDS WITH LARGE LENTICULAR CARBIDES AT THE BORDERS

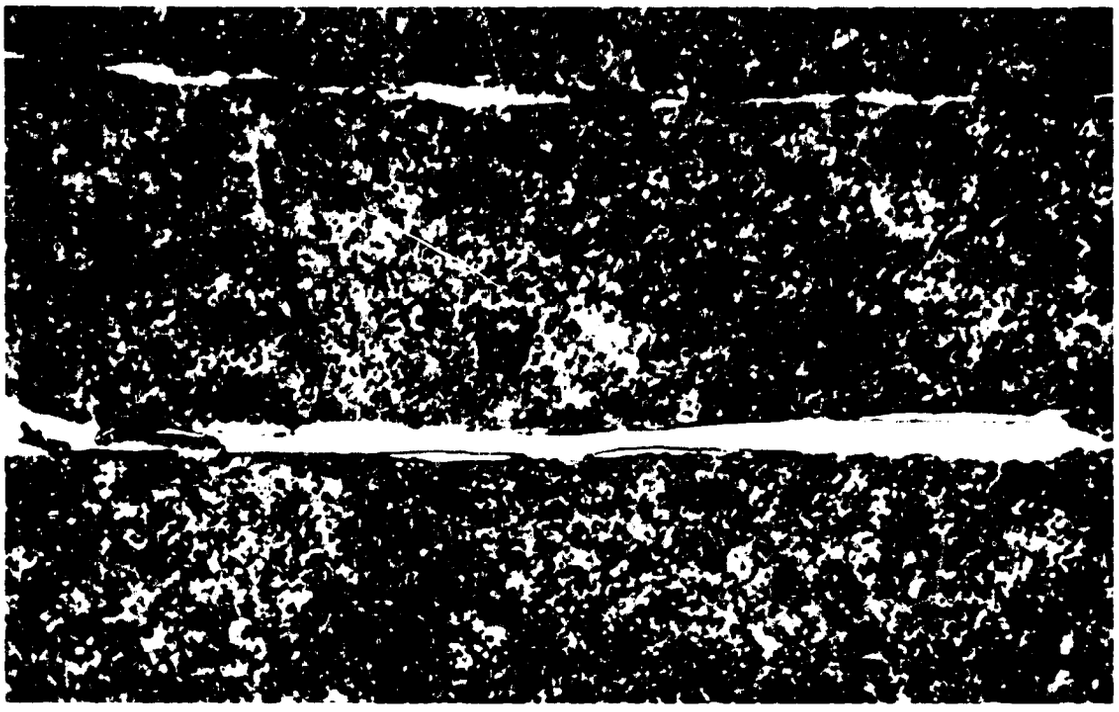

Picral Etch 2000X

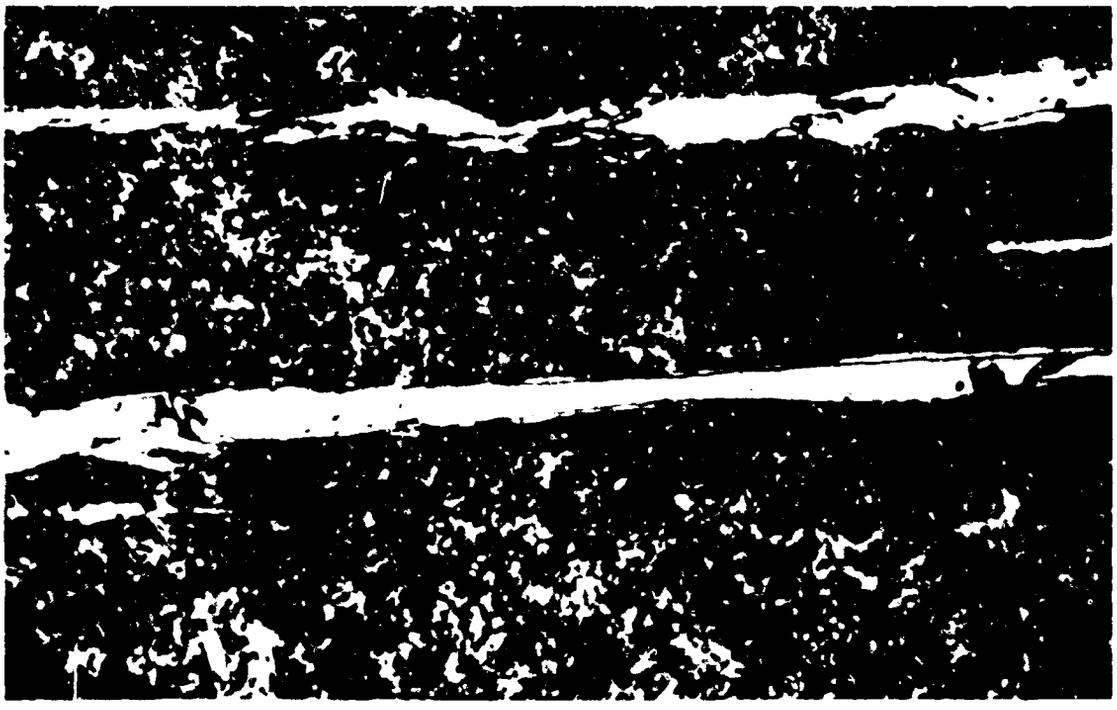

Picral Etch 2000X

Bearing No.891115 Life = 150 Million Revs.

RESEARCH LABORATORY SKF INDUSTRIES, INC.

AL67M050

ENCLOSURE 2

DEFORMATION BANDS BEFORE AND AFTER TEMPERING AT 500°C FOR 1 HOUR

Picral Etch 2000X

The circle was scratched on with a micro-hardness diamond indentor to facilitate relocation of the same area after tempering.

Picral Etch 2000X

Same area as above after tempering in an inert atmosphere.
Circle was removed by repolishing but is shown by black outline.

Brg.No. 891115 Life=150 Million Revs.

RESEARCH LABORATORY SKF INDUSTRIES, INC.

AL67M050

ENCLOSURE 3

CELL STRUCTURES AFTER TEMPERING IN THE ELECTRON MICROSCOPE

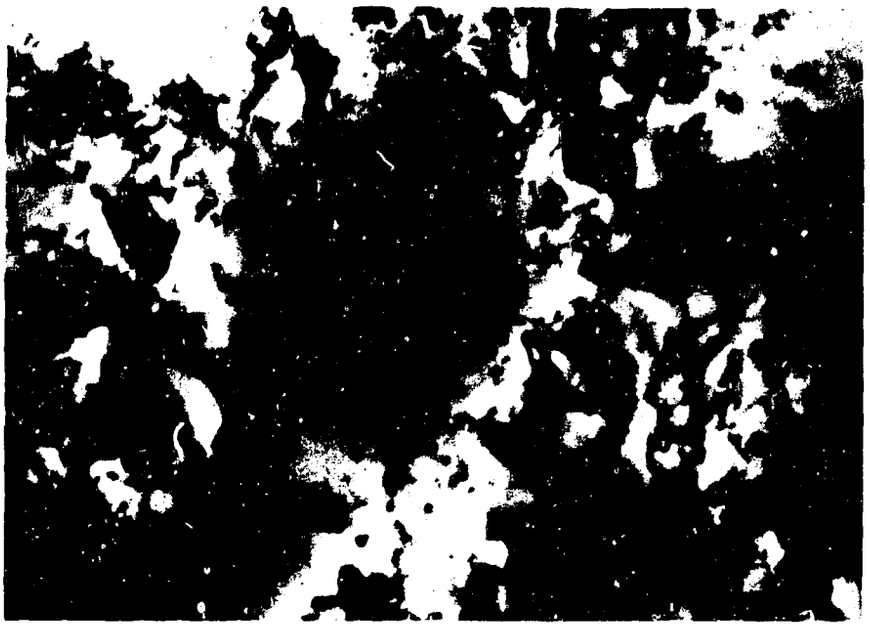

40,000X

Tempered 325°C for 1½ hours. Many small carbide precipitate particles are visible at the cell walls.

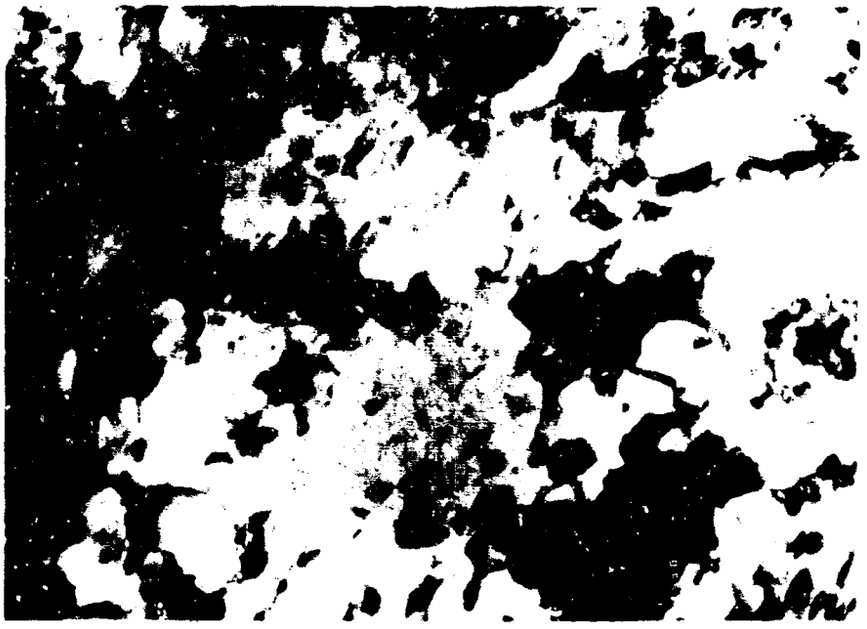

53,000X

Cell structure after tempering at 550°C for 2½ hours. No carbides precipitated in this region during tempering.

AL67M050

ENCLOSURE 4

DEFORMATION BANDS DEVELOPING IN BULK MATERIAL UNDER THE INFLUENCE OF CYCLIC STRESS

Picral Etch 2000X

Deformation bands in their earlier stage of development

Bearing 849-234 Life 157 Million Revs. 52100 steel

Picral Etch 2000X

Deformation bands at a late stage of development

Bearing 849-244 Life 385 Million Revs. CVD 52100 steel

RESEARCH LABORATORY SKF INDUSTRIES, INC.

AL67M050

ENCLOSURE 5

DEFORMATION BANDS PRODUCED IN A SINGLE CYCLE OF LOAD APPLICATION

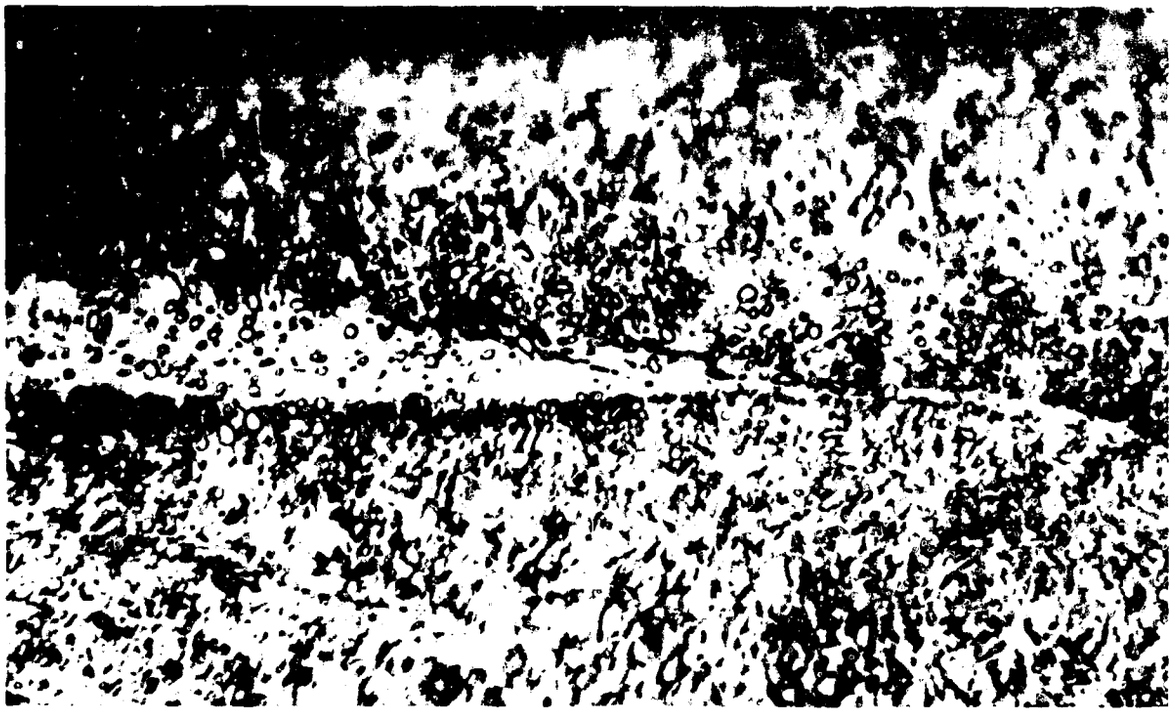

Picral Etch 2000X

The rapidly produced deformation bands, seen as a light etching structure in the vicinity of the cracks, show no evidence of lenticular carbide formation.

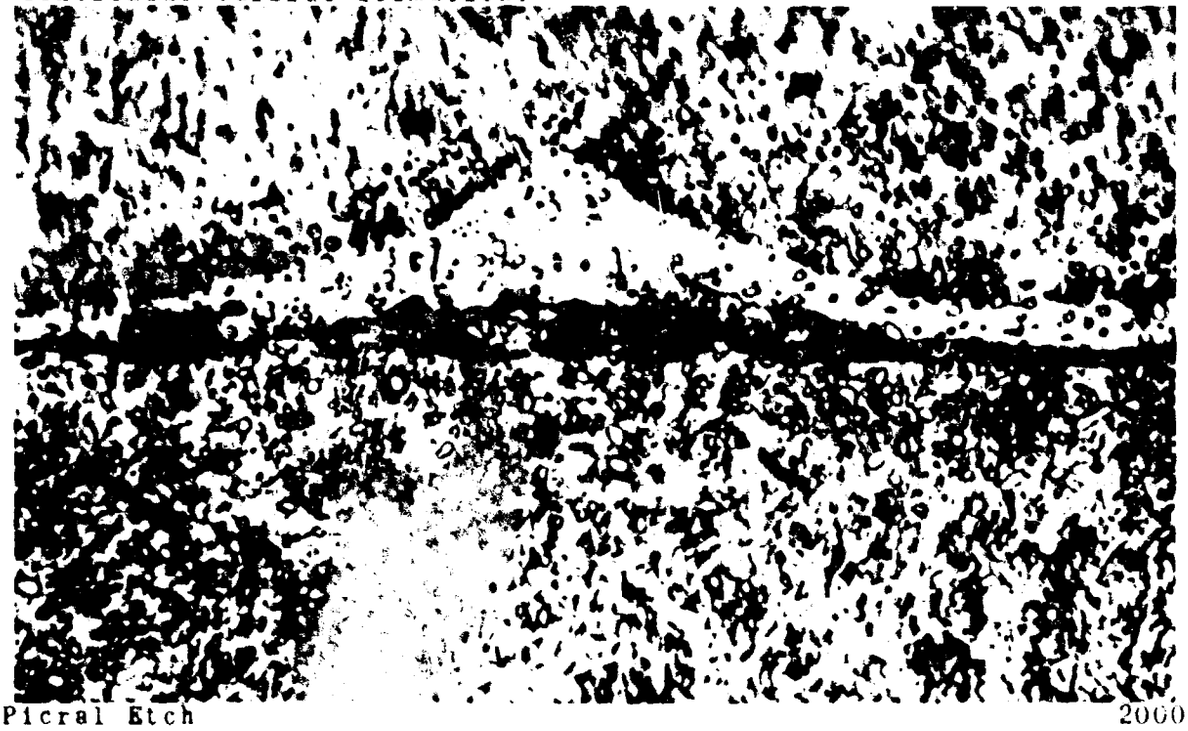

Picral Etch 2000X

AL67M050

ENCLOSURE 6

INCIPIENT SPALL FORMING AROUND A NEAR SURFACE INCLUSION

Unetched 2000X

Cracks associated with the defects and deformation bands.

Picral Etch 2000X

Same area as upper photograph shown etched. Cracking can be seen at the borders of deformation bands.

ENCLOSURE 7

STRESS-INDUCED STRUCTURAL ALTERATION OF MARTENSITE

28000X

A. Unstressed region, tempered martensite

B. Cell

Within deformation bands t
martensitic structure is t
cell structure.

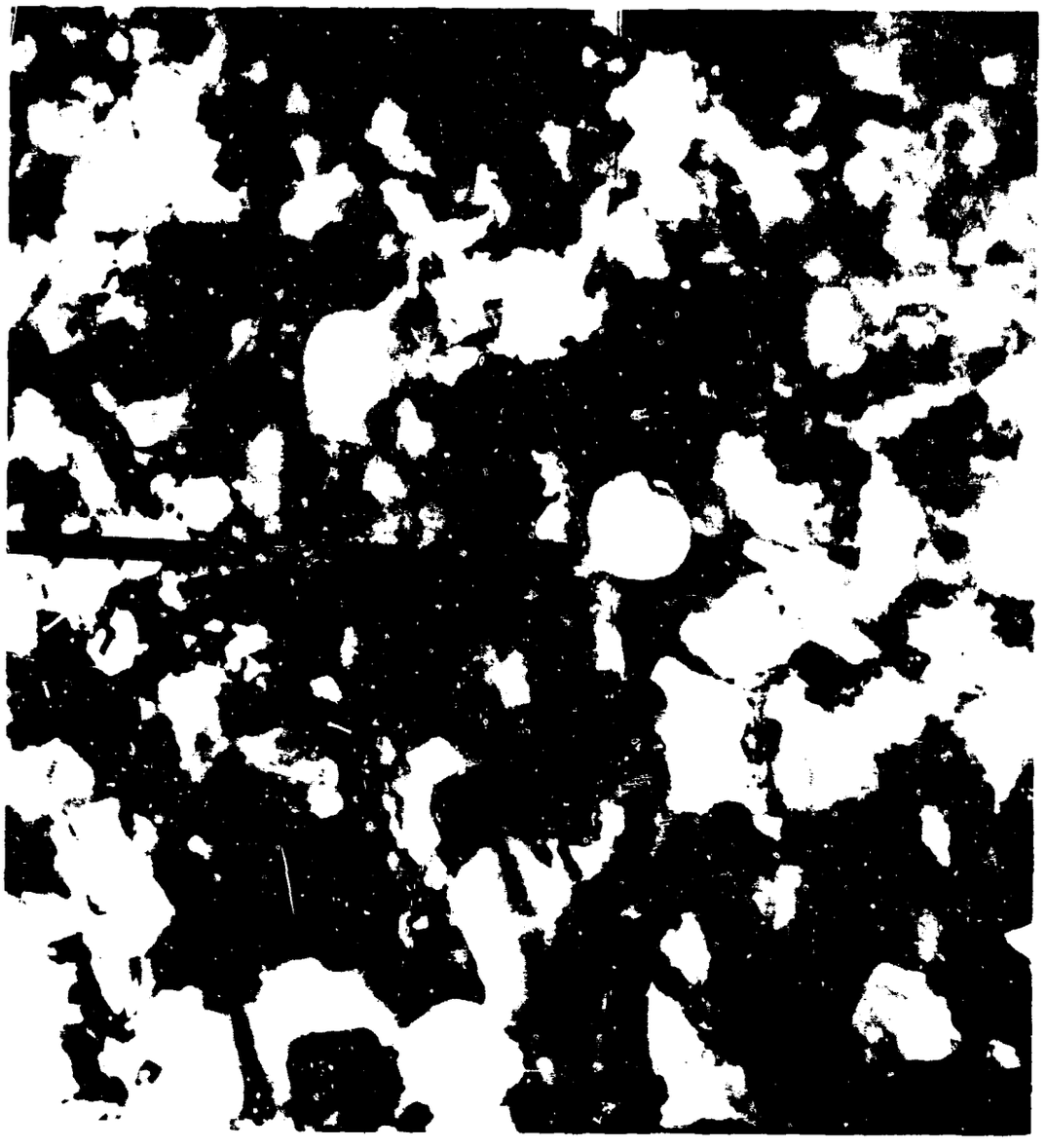

94000X

B. Cell structure produced by cyclic stress

deformation bands the original
itic structure is transformed to a
ructure.

ENCLOSURE 8 AL67M050

CUT AWAY VIEW OF DEEP GROOVE BEARING INNER RING

DEFINING VIEWING SECTIONS

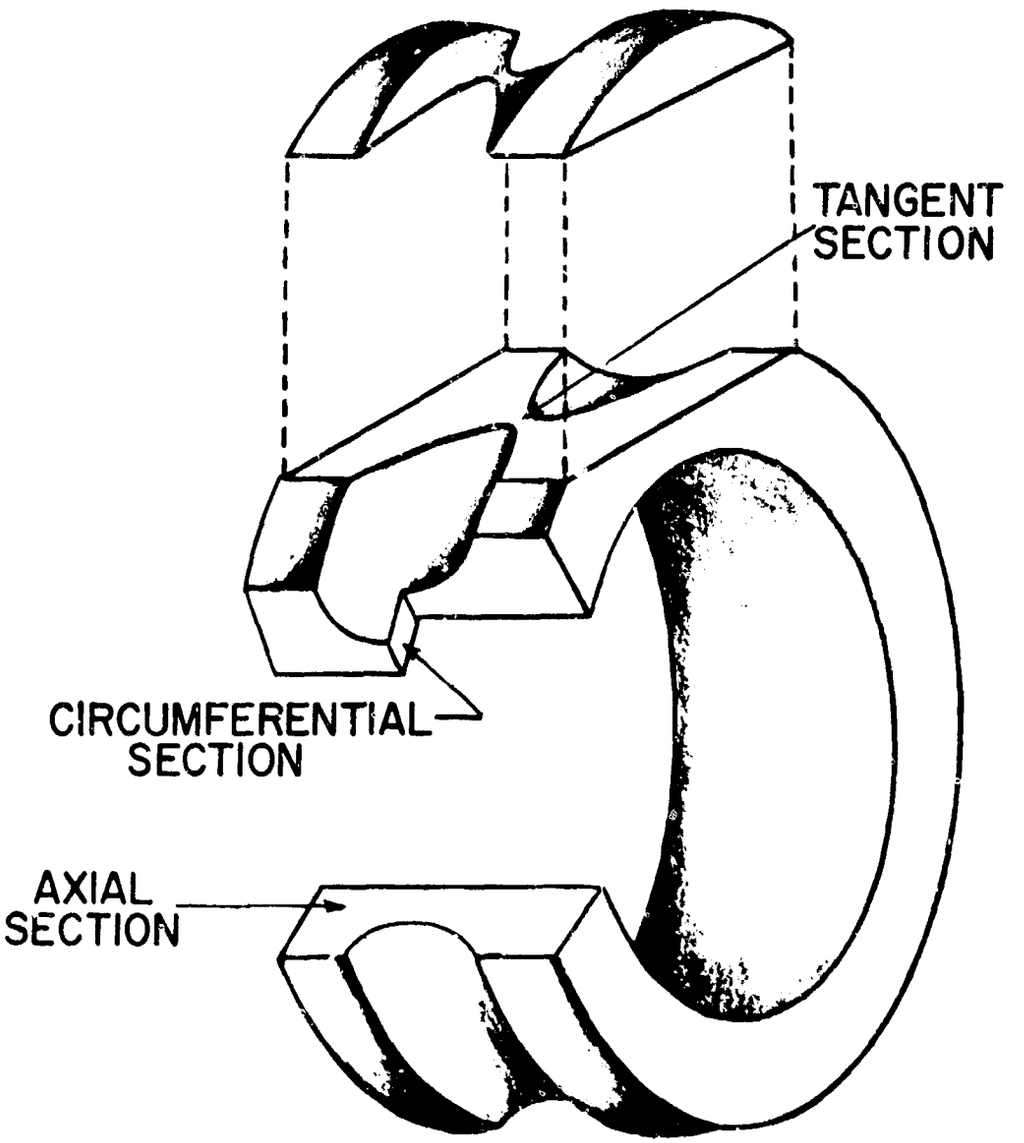

RESEARCH LABORATORY SKF INDUSTRIES, INC.

ENCLOSURE 9

LOW MAGNIFICATION PHOTO OF DEFORMATION BANDS SHOWING THEIR 23° ORIENTATION TO THE SURFACE AS VIEWED ON A CIRCUMFERENTIAL PLANE

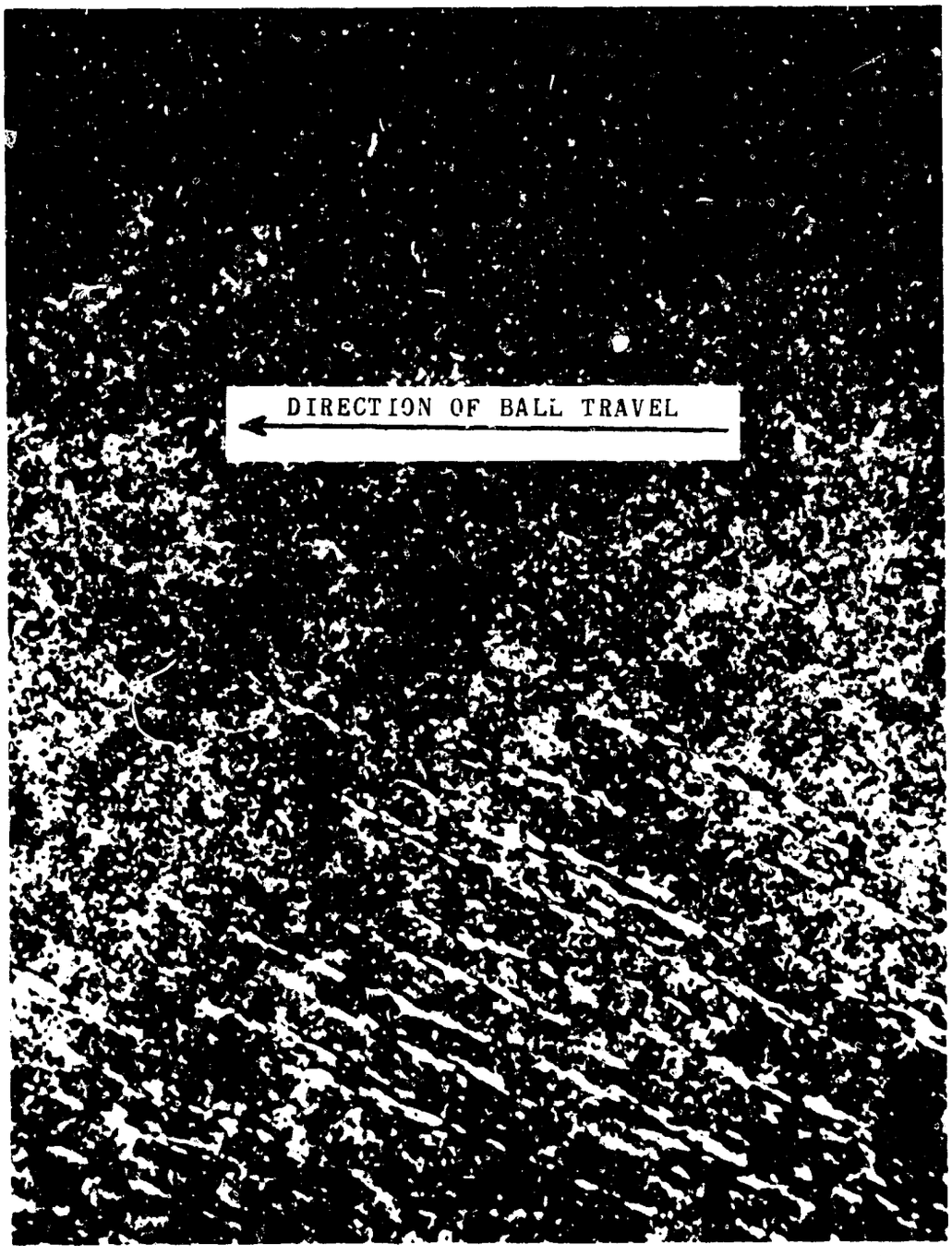

Picral Etch 400X

Bearing 1042-1194 Life 428 Million Revs. 52100 Steel

AL67M050

ENCLOSURE 10

VIEW ON PLANE LYING PARALLEL TO THE PLANE OF THE DEFORMATION BANDS

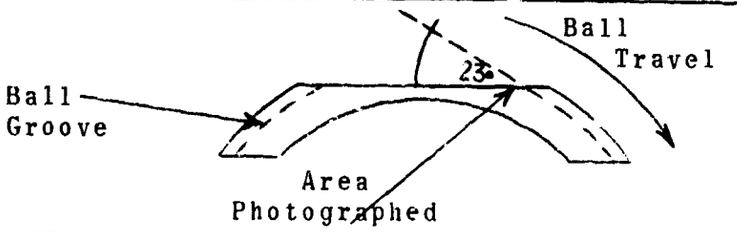

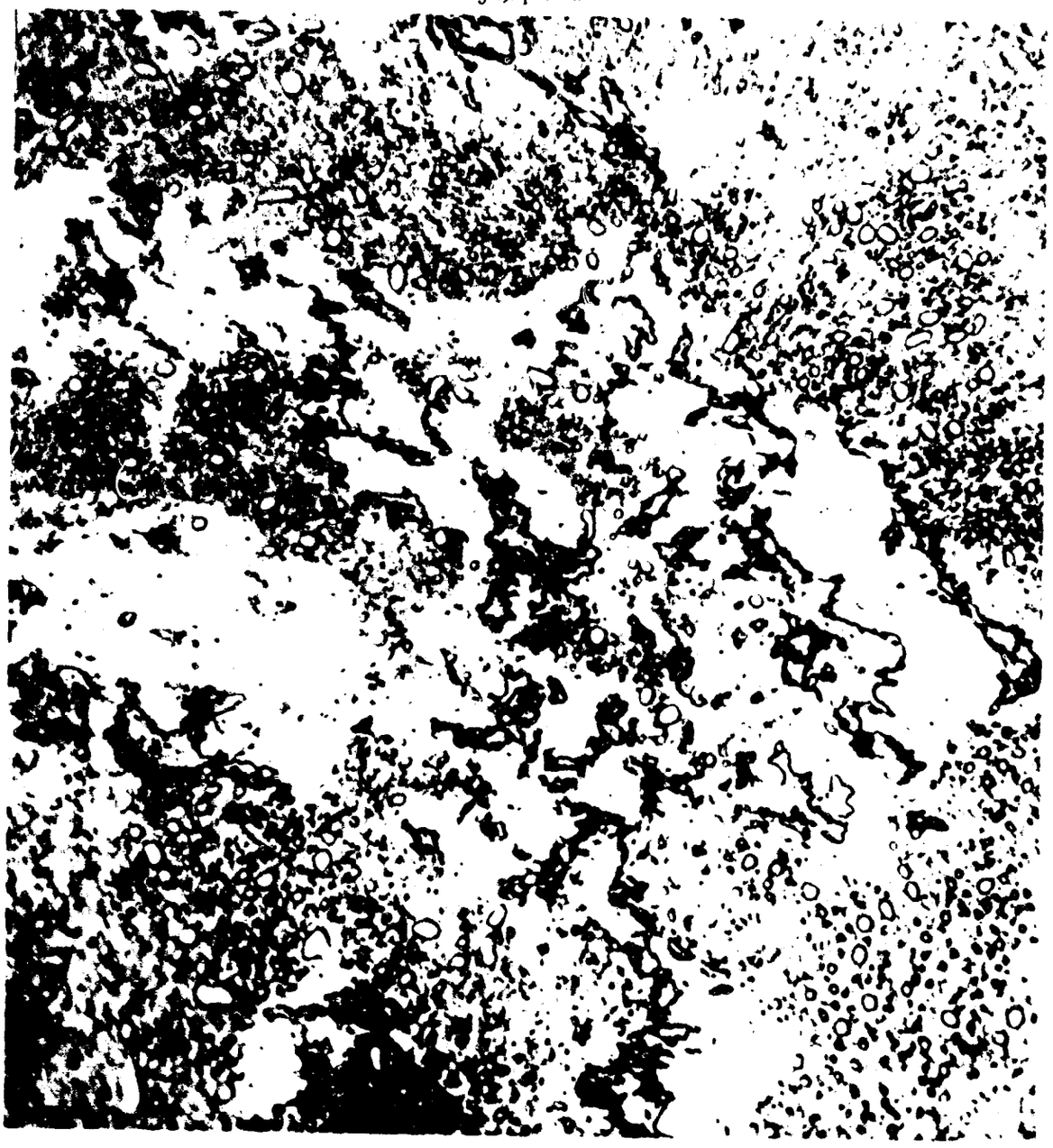

Light Micrograph of Plane Cut 23° to the Ring Groove Tangent–Picral Etch 2000X

RESEARCH LABORATORY SKF INDUSTRIES, INC.

ENCLOSURE 11

CONTACT ELLIPSE ON THE SURFACE OF A 6309 DEEP GROOVE BALL BEARING INNER RING

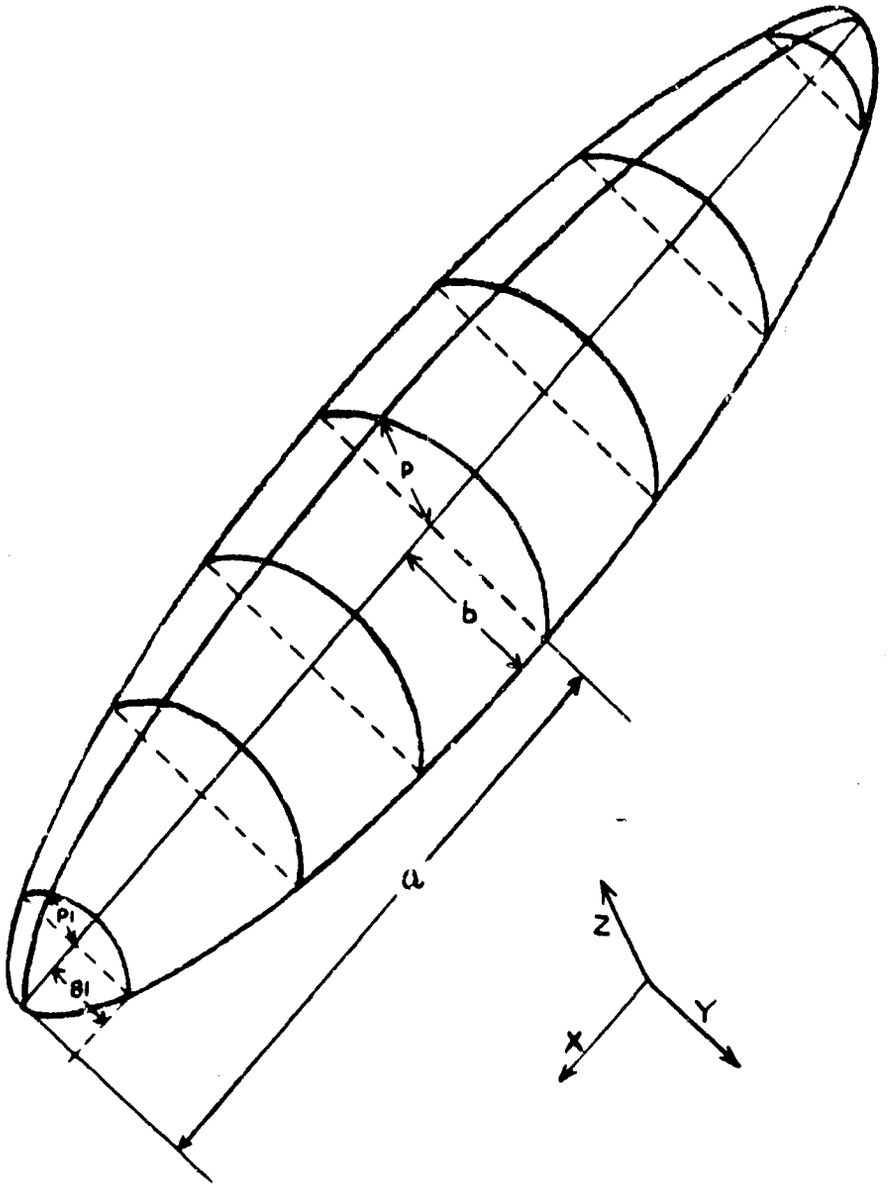

Load - 4240 lbs radial load
Dynamic Capacity to Load Ratio (C/P) - 2.15
Maximum normal Hertzian stress (τmax) = 474,900 psi
Maximum alternating shear stress (τ_{zy} max) = 118,800psi
Depth of max alternating shear stress ($Z_{\tau zy}$max) = 7.6 X 10^{-3} in.
Maximum 45° shear stress (τ max) = 148,000 psi
Depth of max 45° shear stress (Z_o) = 11.7 X 10^{-3} in.
Major and minor semi-axes of contact ellipse

a = 0.1547"
b = 0.01511"

ENCLOSUR

MAXIMUM SHEAR STRESS D

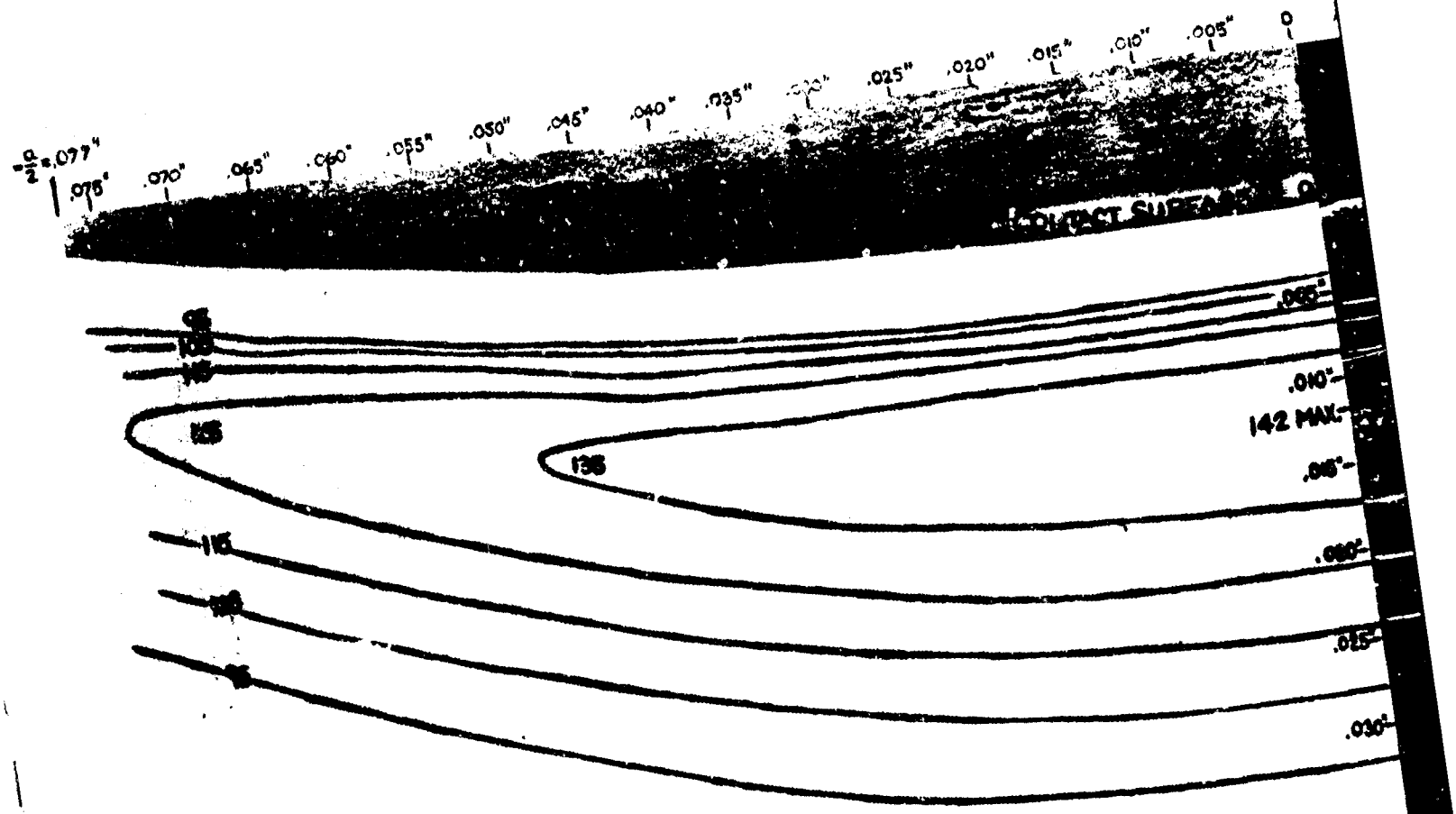

Maximum shear stress distribution (τ 45° ...
loaded as described in Enclosure 9. The c...
maximum shear stress are superimposed on a ...
The horizontal white streaks in the body of ...
Values shown on the contour lines are τ ma...
below the contact surface is shown on the ...
line at the contact surface is an artifact ...

ENCLOSURE 12

AL67M050

STRESS ON AN AXIAL PLANE

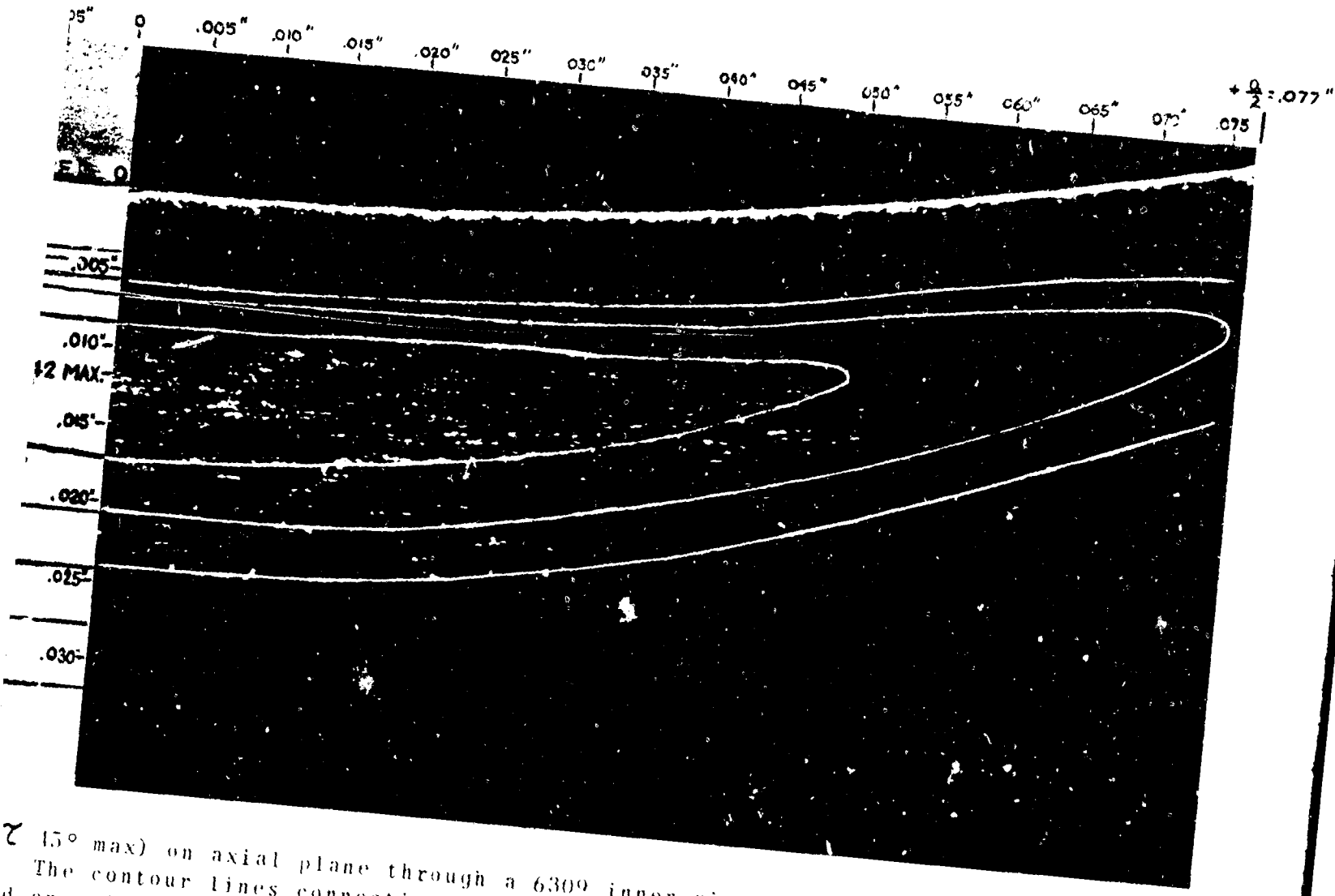

τ 15° max) on axial plane through a 6309 inner ring
• The contour lines connecting points of equal
ed on a 100X microphotograph of an actual specimen.
; body of the specimen are deformation bands.
ire τ max values in thousands of psi. Distance
on the depth scale at the center. (The white
rtifact due to reflected light).

100X

2

ENCLOSURE 13

INCIPIENT SPALL INITIATED AT A LARGE NON-METALLIC INCLUSION

80X
Low magnification photo of bearing surface showing incipient spall

800X
Surface view of cracked area after polishing and etching. A large silicate type inclusion can be seen at the base of the crack. Deformation bands along the crack are evident.

Brg. No. 693137 Life = 406 Mill. Revs.

AL67M050

ENCLOSURE 14

EXAMPLES OF DEFORMATION BANDS FORMING AT SMALL NON-METALLIC INCLUSIONS

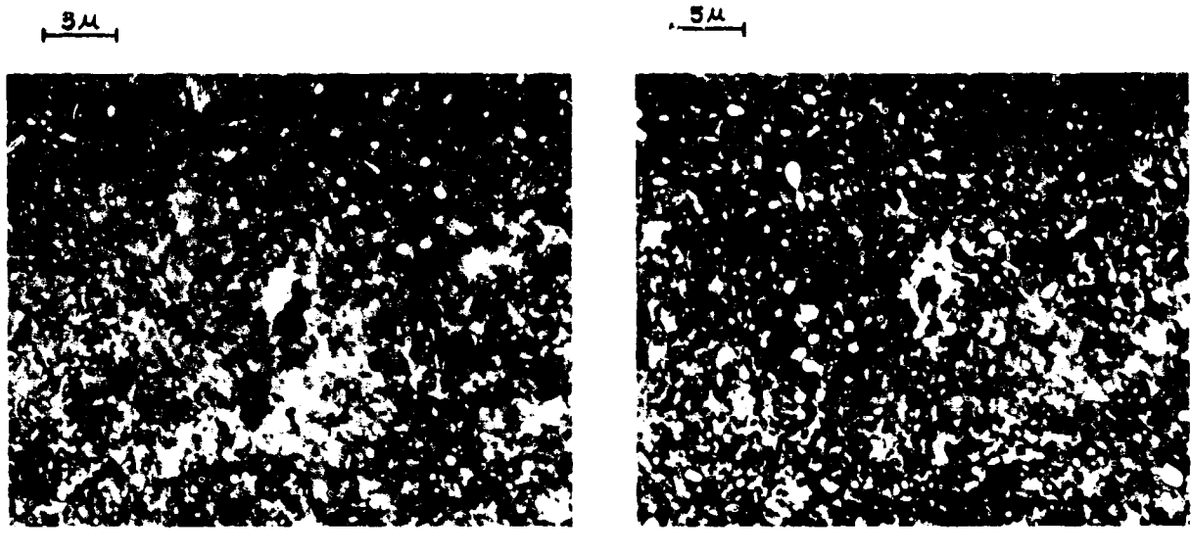

Picral Etch

2000X

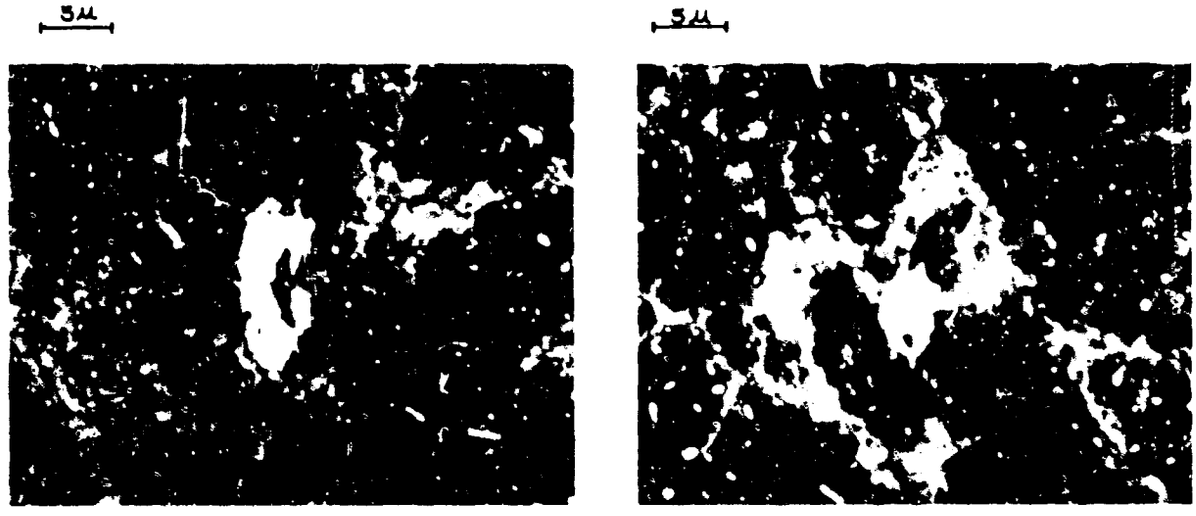

Picral and Sodium
Tridecylbenzene sulfonate
etch

2000X

Addition of a wetting agent to Picral etch develops the prior austenite grain boundaries in the structure.

All micrographs were taken from specimen 1042-1134, life 77 million revolutions, Airmelt 52100 steel Fully stabilized -0% austenite.

AL67M050

ENCLOSURE 15

SURFACE VIEW OF A GRINDING FURROW ON AN ENDURANCE TESTED INNER RING

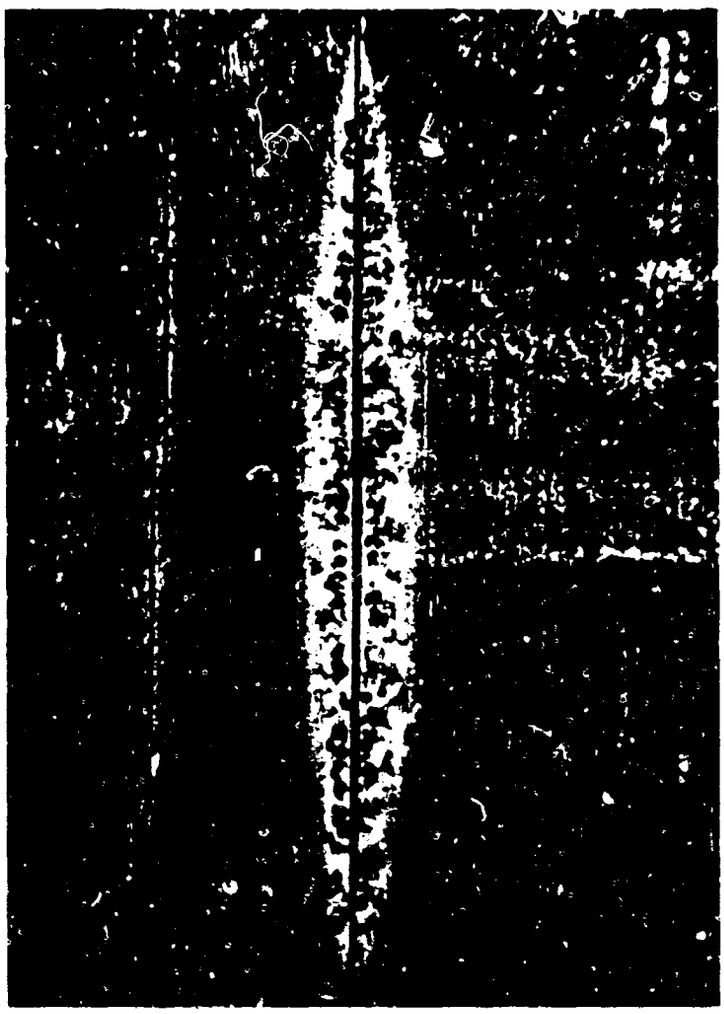

100 X

Surface distress is apparent in the glazed area surrounding the furrow after 150 million revs.

ENCLOSURE 16

SURFACE DISTRESS SIMILAR TO THAT SHOWN IN ENCLOSURE 15

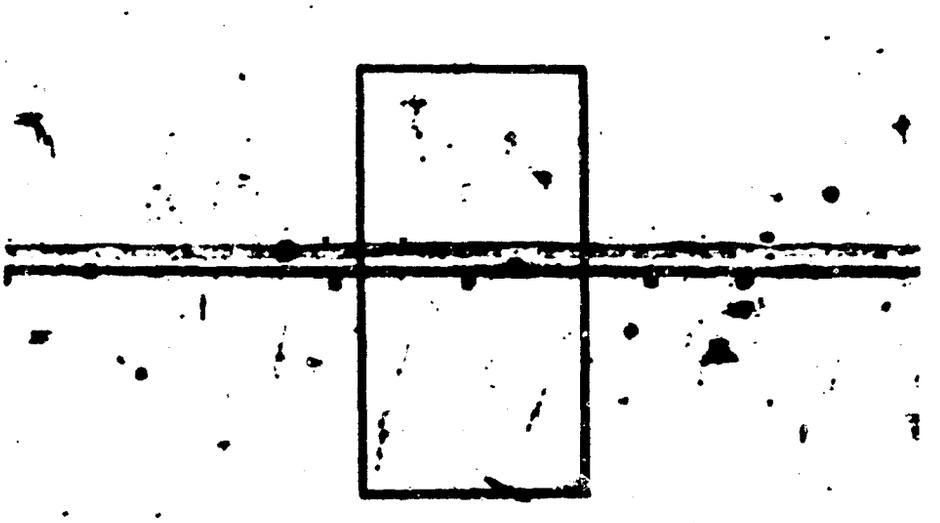

400X

Polishing to a depth of .0001" reveals cracking under the glazed and pitted area which surrounds a furrow.

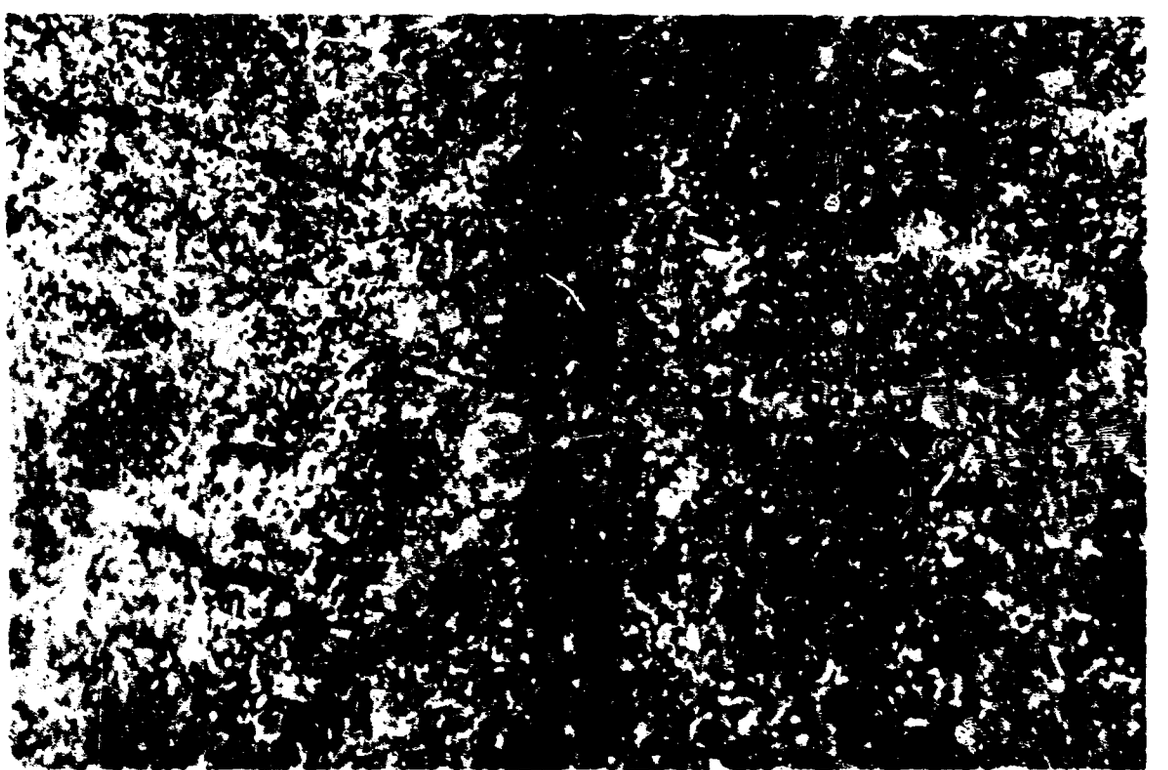

Picral Etch 1000X

Area outlined above is shown rotated 90° at higher magnification in the etched condition.

AL67M050

ENCLOSURE 17

ORIGINAL CONTACT SURFACE POLISHED TO A DEPTH .0002" BELOW A GRINDING FURROW

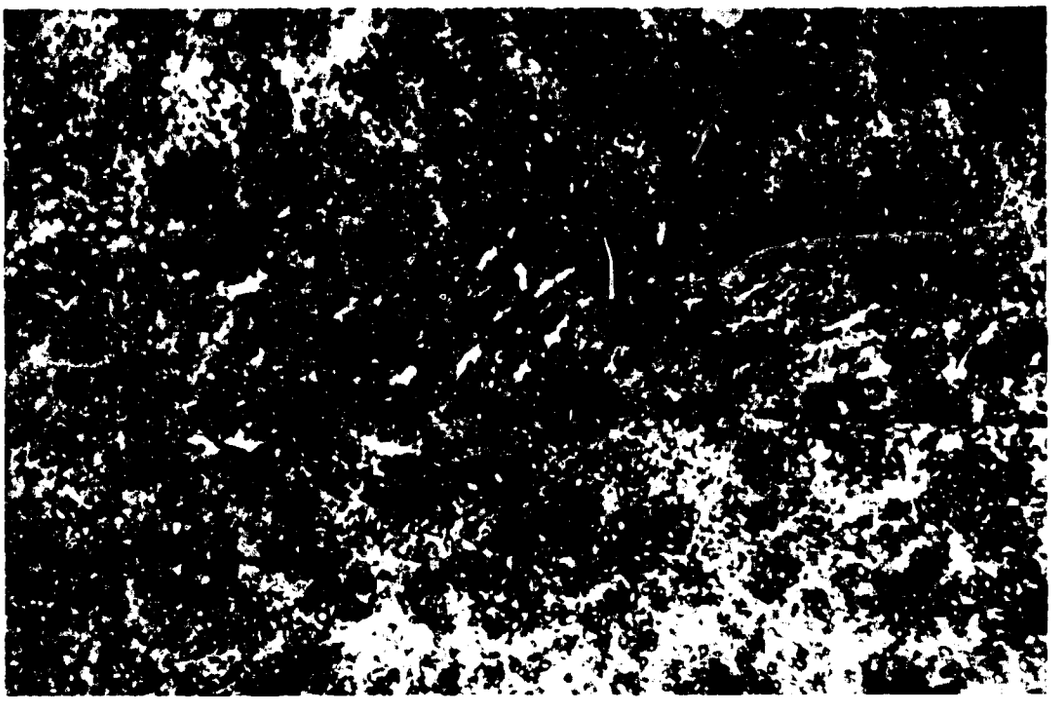

Picral Etch 1000X

Deformation bands are evident on both sides of a furrow shown by a dotted line. The original furrow was removed by polishing.

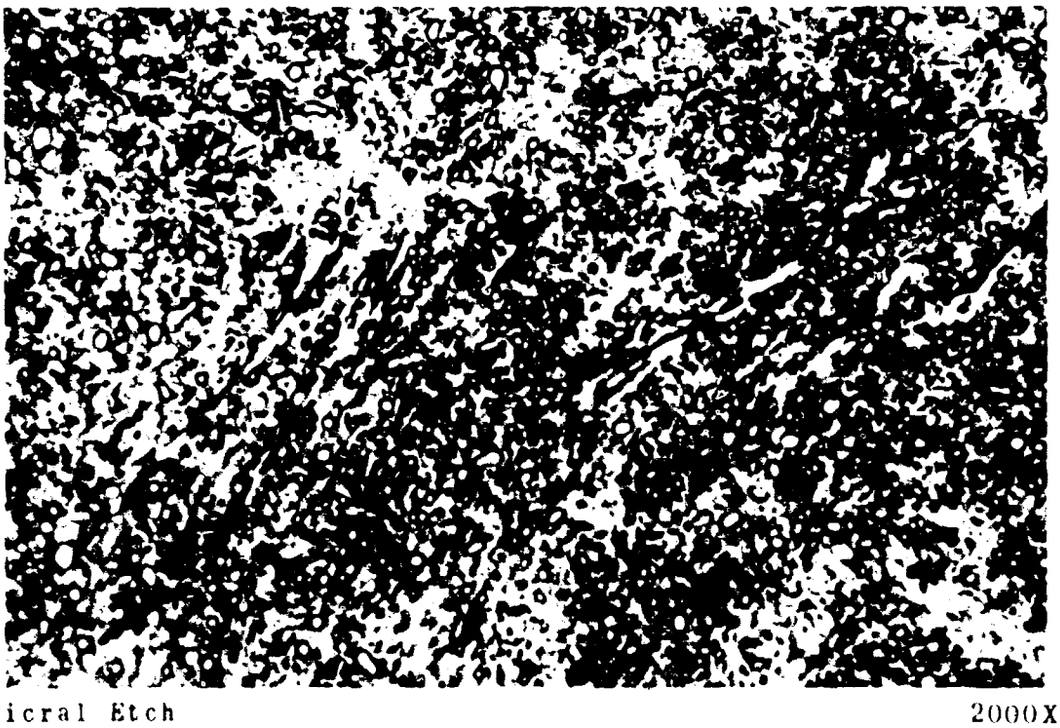

Picral Etch 2000X

High magnification details of deformation around furrows. The presence of lenticular carbides indicates that the deformation took place over a long period of cycling. (Bearing No.693137 Life=406 Mill.Revs.)

AL67M059

ENCLOSURE 18

INCIPIENT SPALLING UNDER A FURROW THAT WAS POLISHED AWAY

SURFACE SHOWN IS .0002" BELOW ORIGINAL CONTACT SURFACE & SHOWS DEFORMATION BANDS

Picral Etch 1000X

RESEARCH LABORATORY SKF INDUSTRIES, INC.

AL67M050

ENCLOSURE 19

FULL SCALE SPALL INITIATED AT THE SURFACE BY A GRINDING FURROW

Schematic showing relative positions of the circumferential cutting plane (shown below), the grinding furrow and the shallow end of the spall.

10X

Furrow Initiated Spall

100X

Circumferential plane showing the area where the grinding furrow leads into the spall. The shallow entry into the spall can be seen to follow the direction of locally produced deformation bands lying near the original contact surface.

AL67M050

ENCLOSURE 20

SURFACE PHOTOGRAPHS SHOWING INCIPIENT SPALLING CAUSED BY SURFACE DISTRESS AROUND A DEBRIS DENT

200X

Original Unpolished Contact Surface

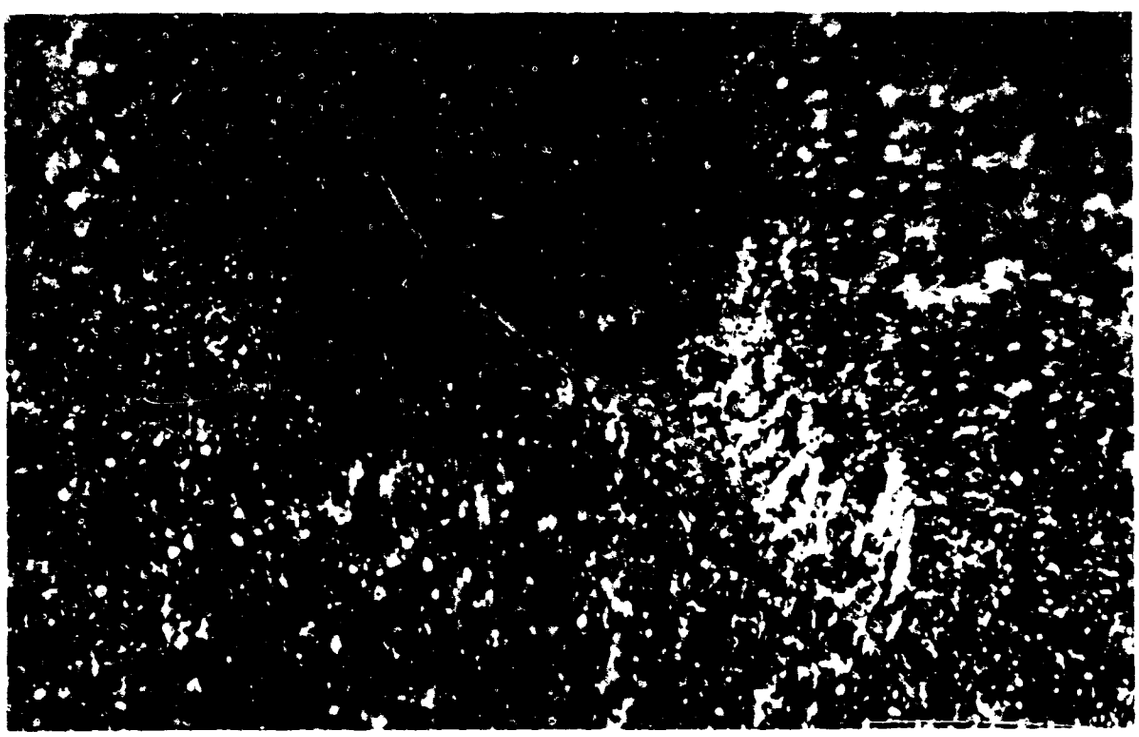

Picral Etch 1000X

Same surface after polishing to a depth of .0002". A partial outline of the dent has been drawn in dotted line. Deformation bands form under the glazed area, not under the dent itself.

Bearing No. 707501 Life=302 Million Revs.

RESEARCH LABORATORY SKF INDUSTRIES, INC.

AL67M050

ENCLOSURE 21

SURFACE AND SUBSURFACE DAMAGE ASSOCIATED WITH PITS

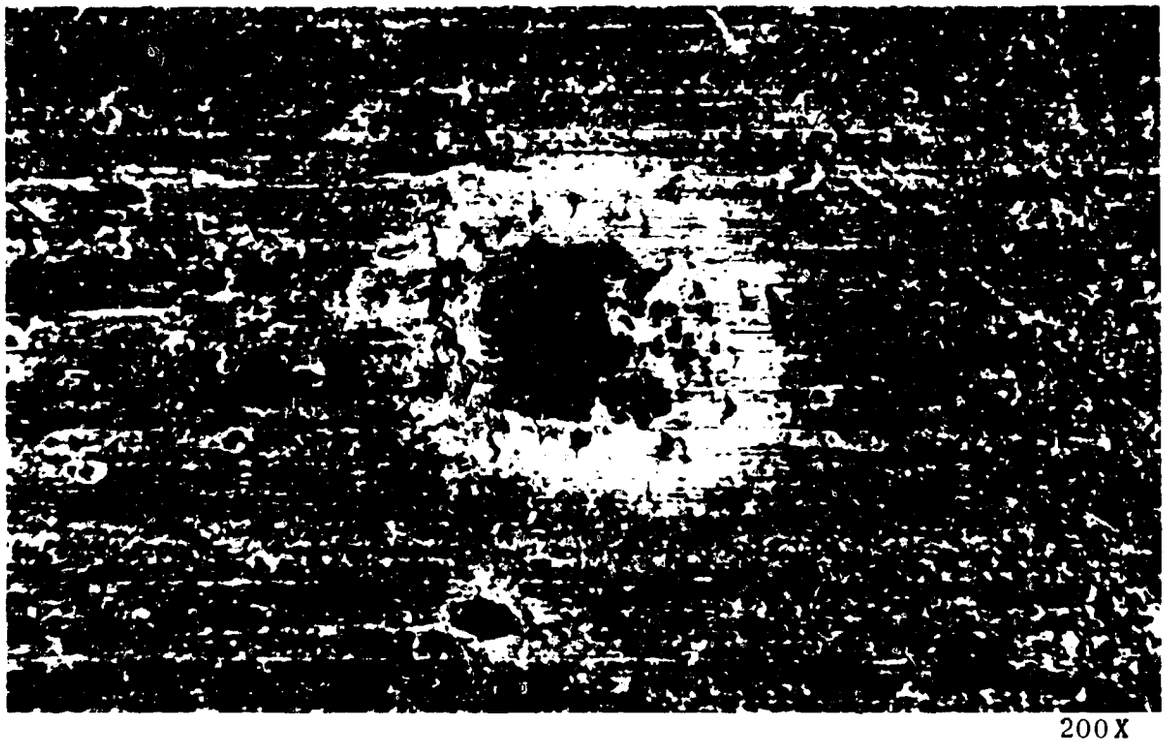

200X

Original unpolished contact surface

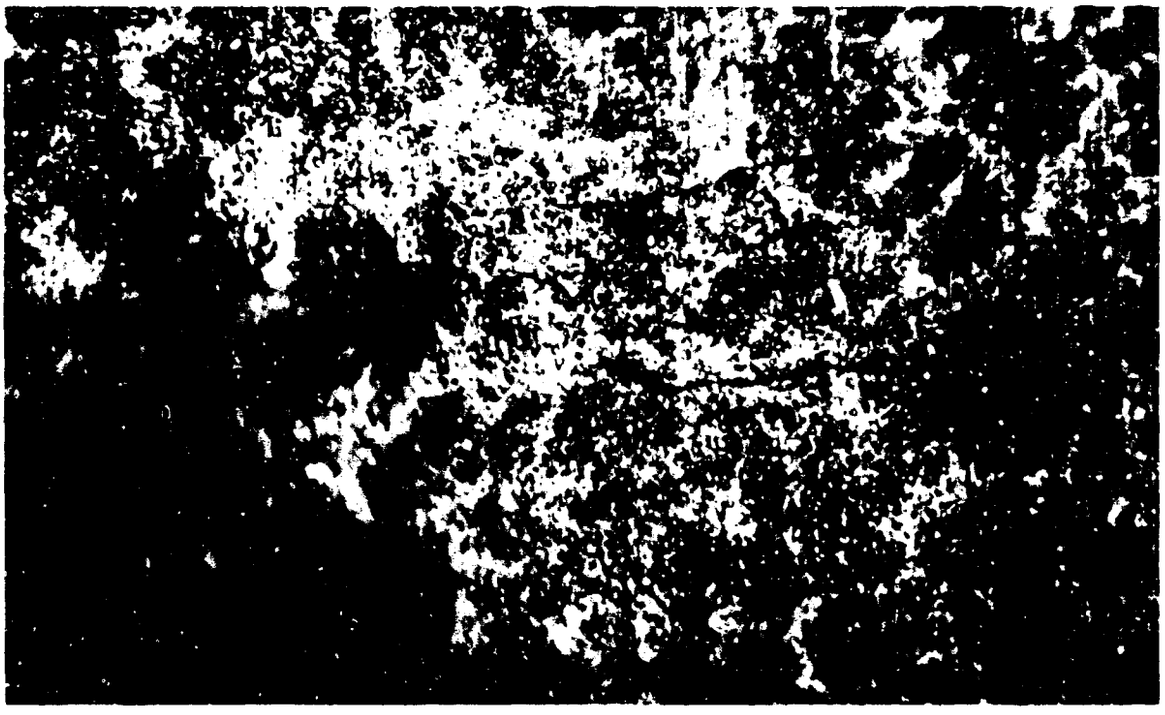

1000X

Polishing to a depth of .0001" below original surface reveals cracks in glazed area.

Brg. No. 707142 Life=120 Mill. Revs.

RESEARCH LABORATORY SKF INDUSTRIES, INC.

AL67M050

ENCLOSURE 22

SPALLING AT AN INTENTIONALLY PRODUCED SCRATCH

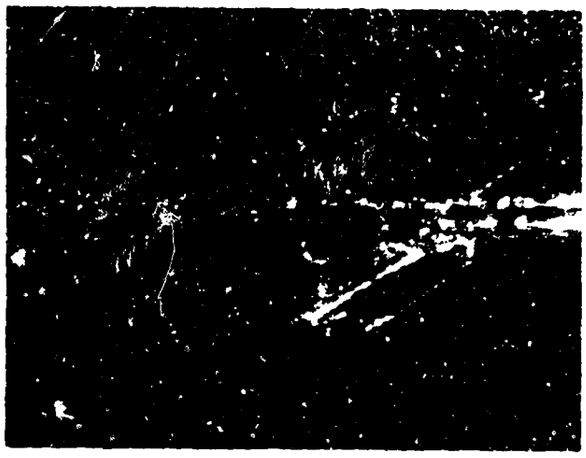

20X

Intentionally produced scratch running across the groove (perpendicular to the rolling direction) of a bearing inner ring.

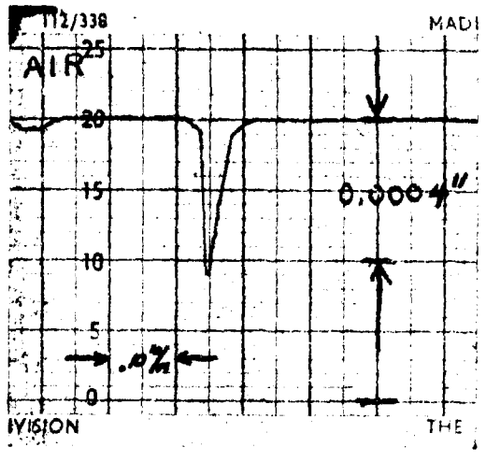

Talysurf trace through the scratch shows it to be approximately 0.0004" deep.

Rolling Direction

10X

Same scratch after the bearing failed. The scratch remains intact with the spall directly behind it, in the rolling direction.

Bearing No. 110130

12.8 Million Revolutions

RESEARCH LABORATORY SKF INDUSTRIES, INC.

ENCLOSURE 23 AL67M050

SPALLS INITIATED AT GOUGES THAT WERE INTENTIONALLY PRODUCED TO SIMULATE DENTS

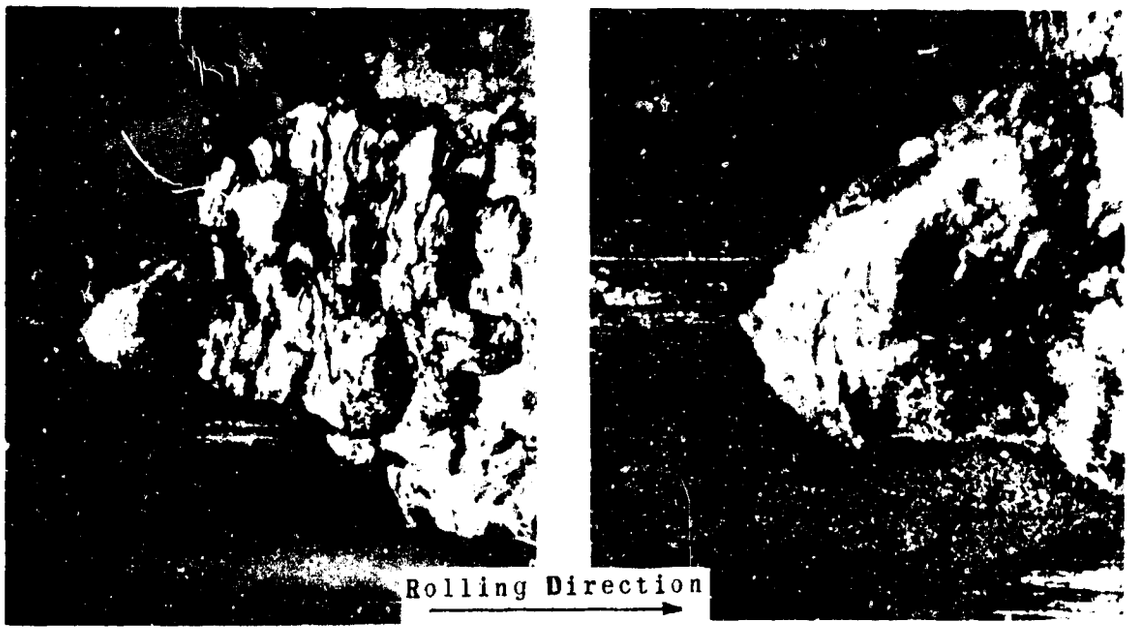

10X 20X

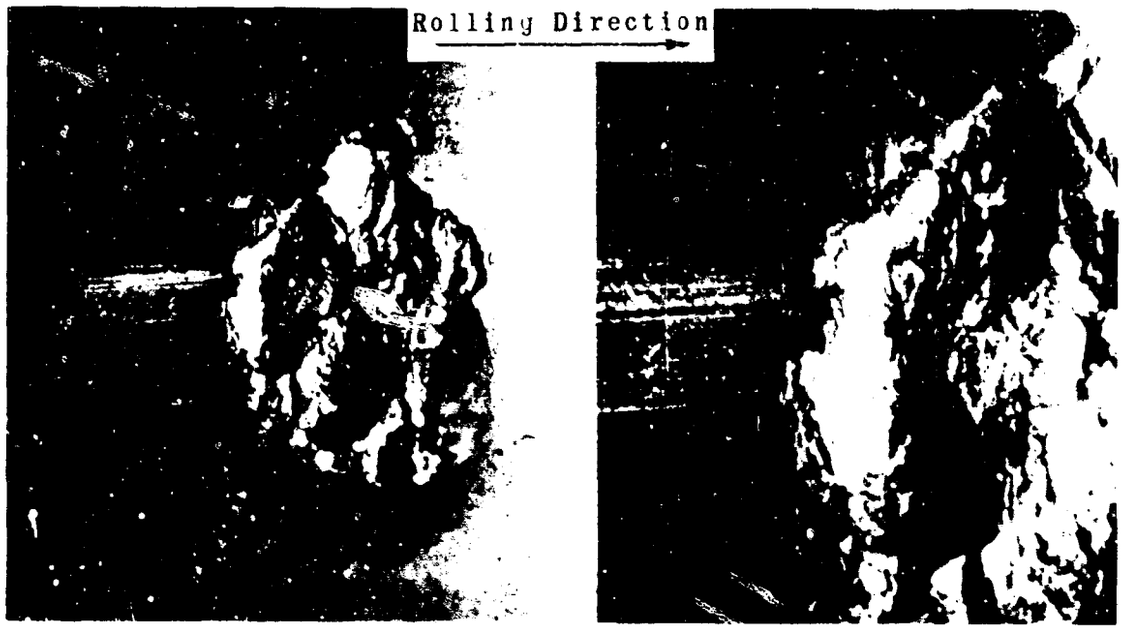

10X 20X

High and low magnification views show that the defect remains intact and that failure is initiated under the glazed areas surrounding the defects.

AL67M050

ENCLOSURE 24

EXAMPLES OF SPALLS INITIATED AT GRINDING MARKS

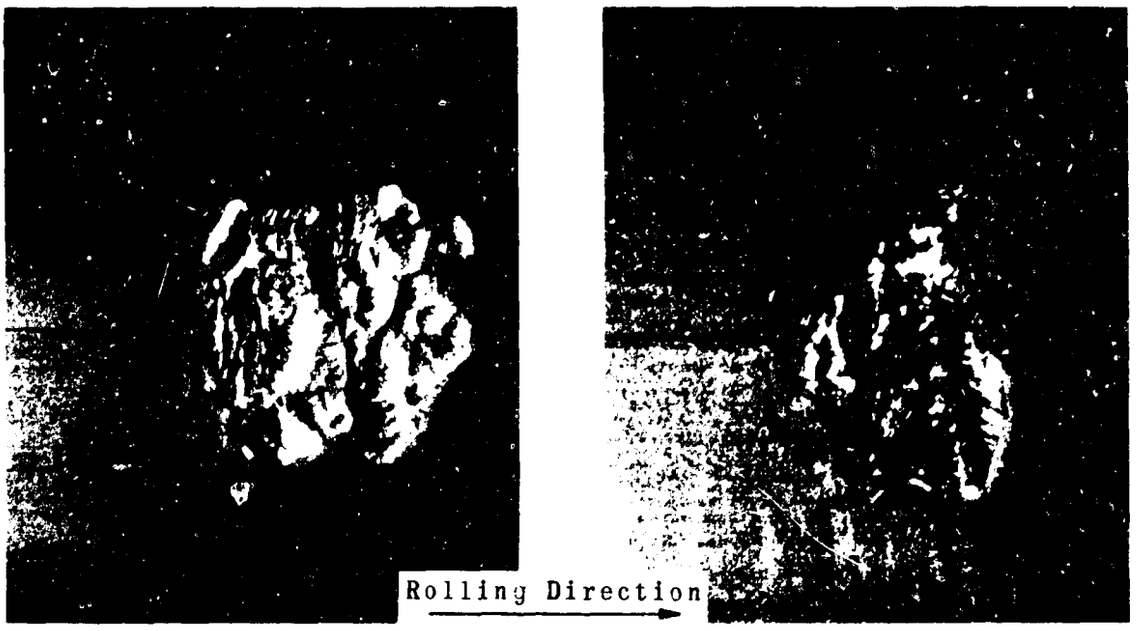

10X 10X

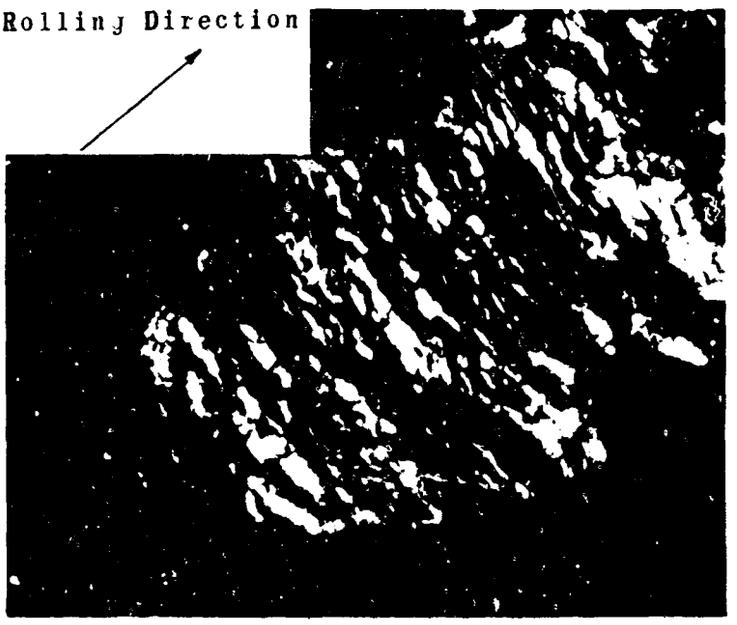

15X

All three spalls show the typical shallow slope at the ball entry end of the spall. Direction of ball travel is shown, i.e. the ball always rolls over the shallow end of the spall first. Depth perception effects are enhanced in the lower photograph by placing the light source at an extremely oblique angle.

AL67M050

ENCLOSURE 25

SURFACE ORIGINATED FATIGUE FAILURES EXAMPLES OF SPALLS INITIATED AT DENTS

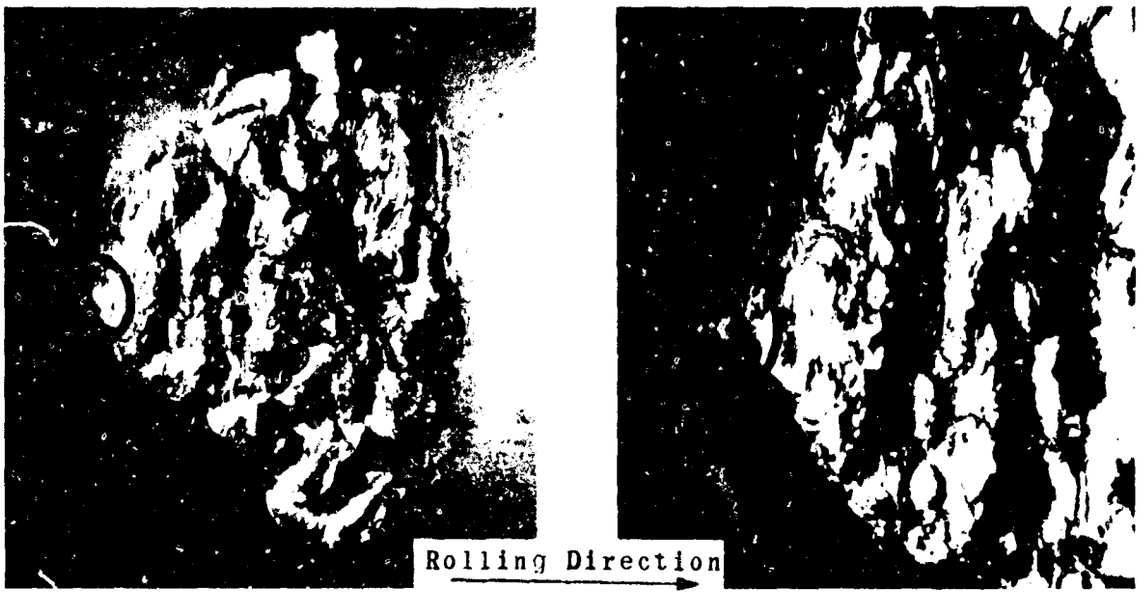

10X 20X

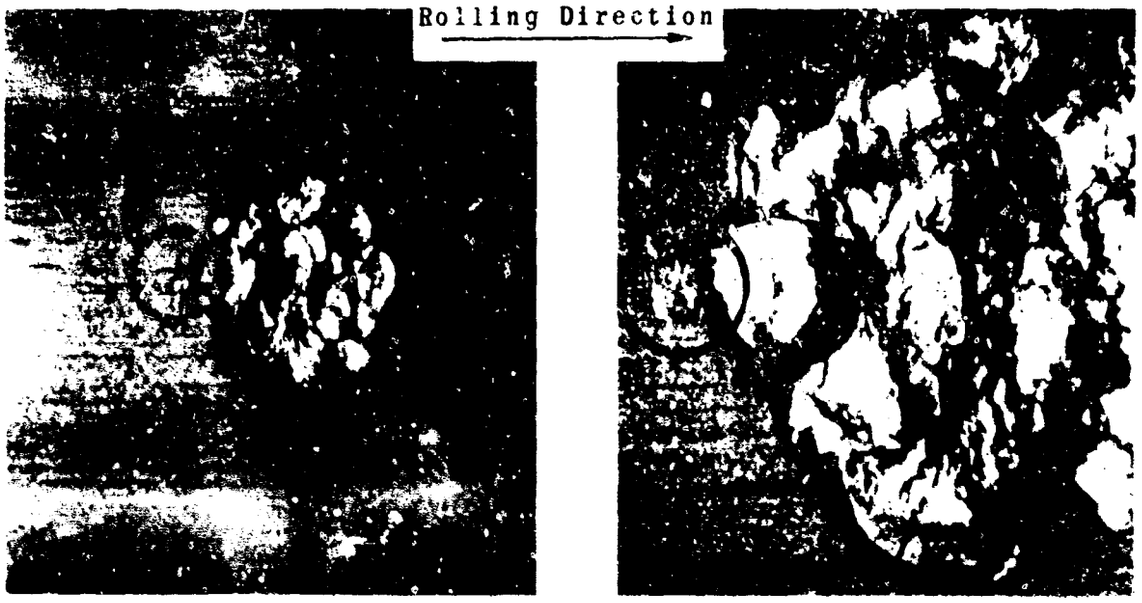

10X 20X

Same spalls shown at low and higher magnification. Dent initiation points shown circled. Lighting condition cause the glazed areas to appear as dark zon

RESEARCH LABORATORY SKF INDUSTRIES, INC.

ENCLOSURE 26

EXAMPLES OF SPALLS INITIATED AT "PITS"

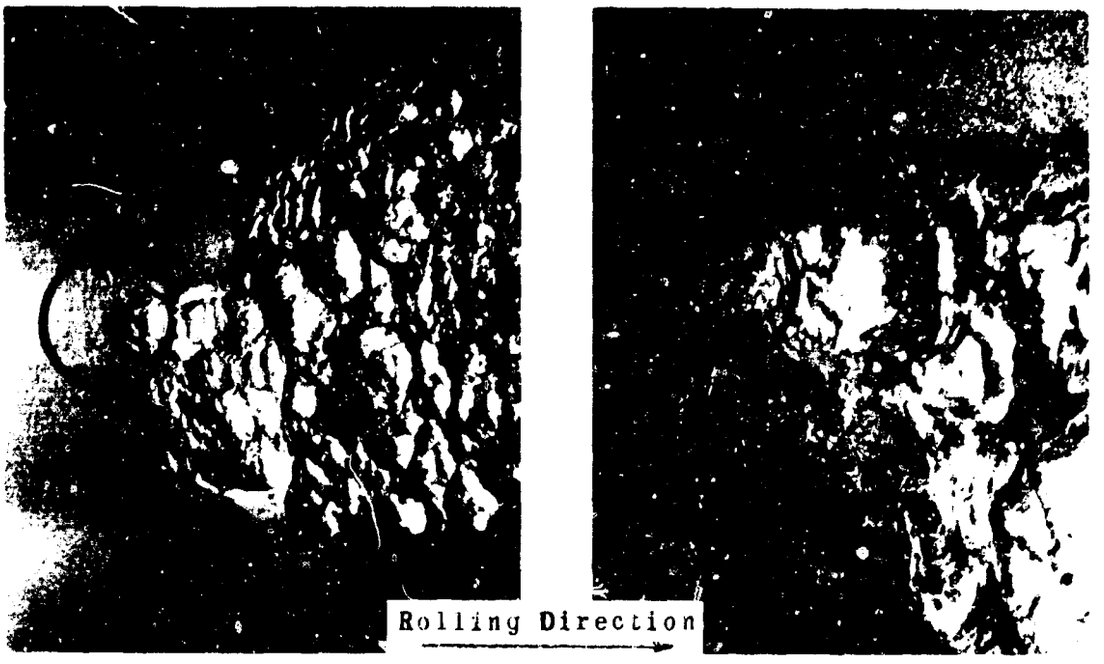

10X 20X

Low and higher magnification viewsof a "pit that initiated failure. Pits tend to have an irregular outline and a roughened bottom while dents tend to look like a depression in the original surface

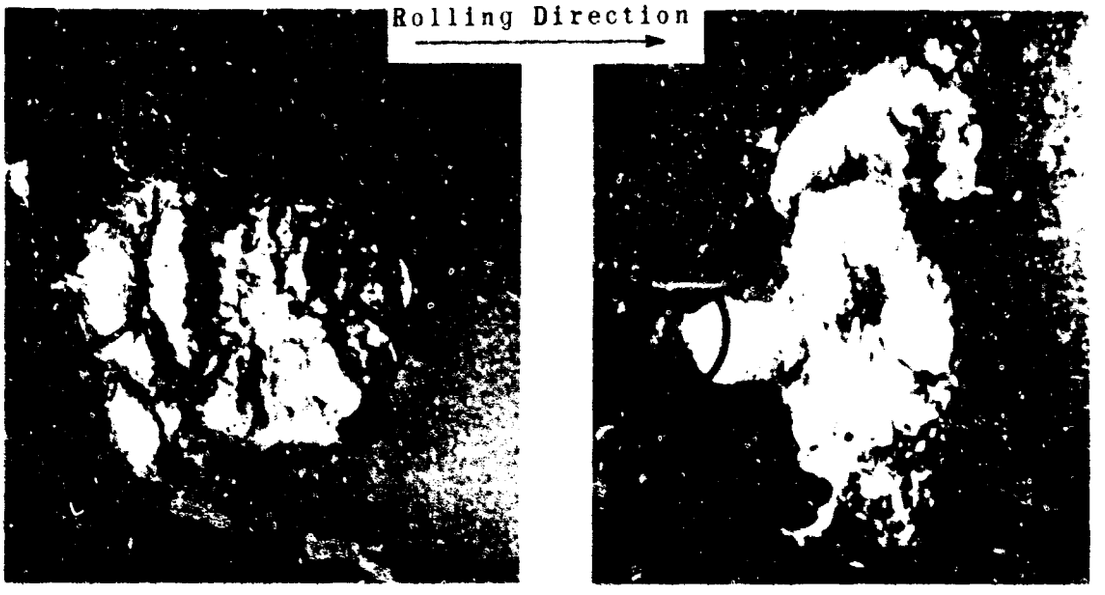

10X 10X

Examples of spall initiation points that show characteristics of both pits and dents.

AL67M050

ENCLOSURE 27

FATIGUE FAILURES OF UNDETERMINED ORIGIN

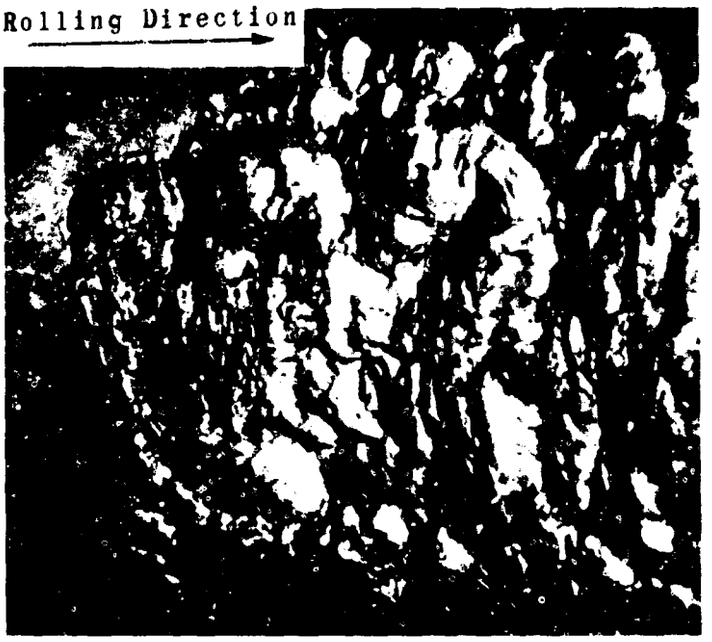

10X

Spall with a shallow ball entry end, believe to be surface originated although no surface defect is evident.

10X

Same type of spall as above.

10X

Spall with steep slopes at each end. Subsurface initiation at a non-metallic is suspected.

ENCLOSURE 28

ELECTRON FRACTOGRAPHS FROM A SPALLED SURFACE

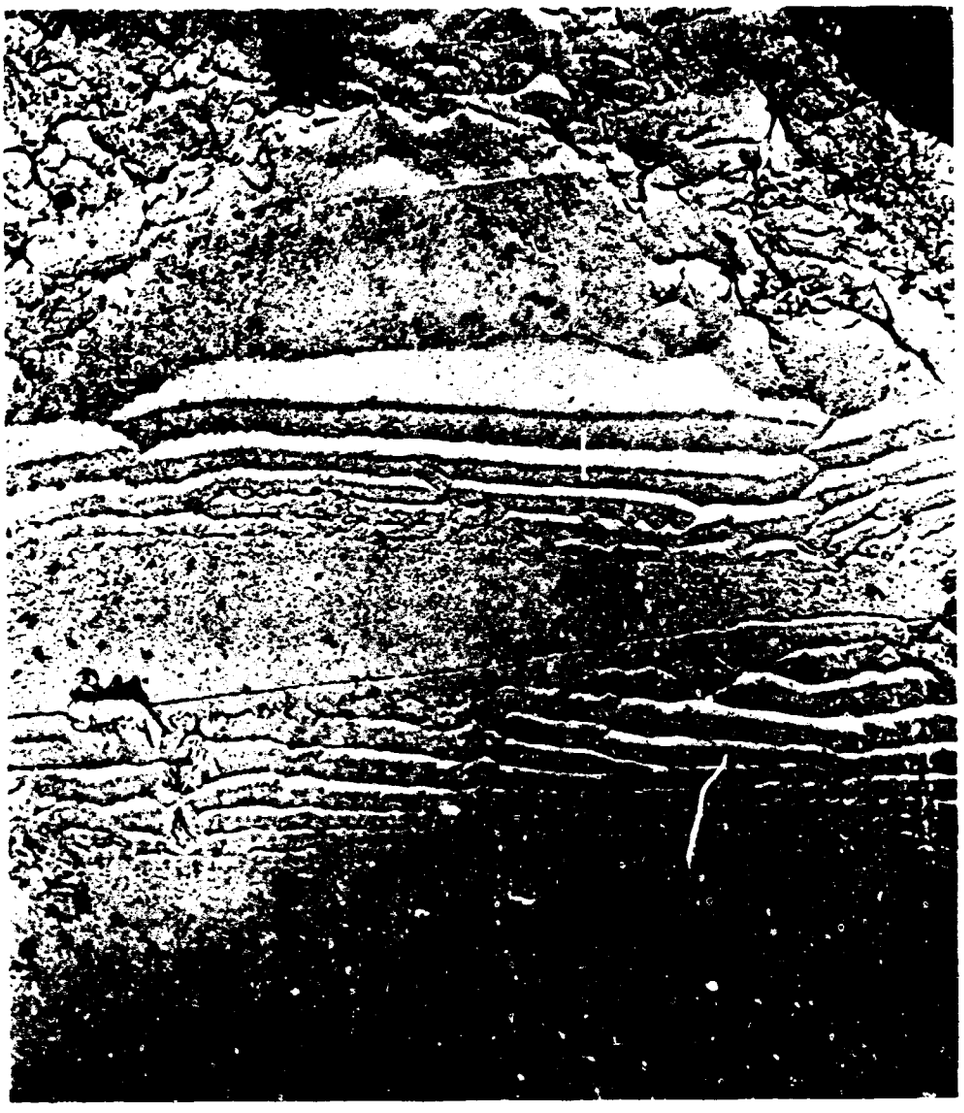

29,000X

Cleavage surface indicating brittle type fracture

ENCLOSURE 29

ELECTRON FRACTOGRAPH FROM A SPALLED SURFACE

28,000X

Fatigue striations around a second phase particle

ENCLOSURE 30

ARRANGEMENT OF TEST SPECIMEN AND ULTRASONIC MONITORING HEAD

IN SKF FLAT WASHER TESTER

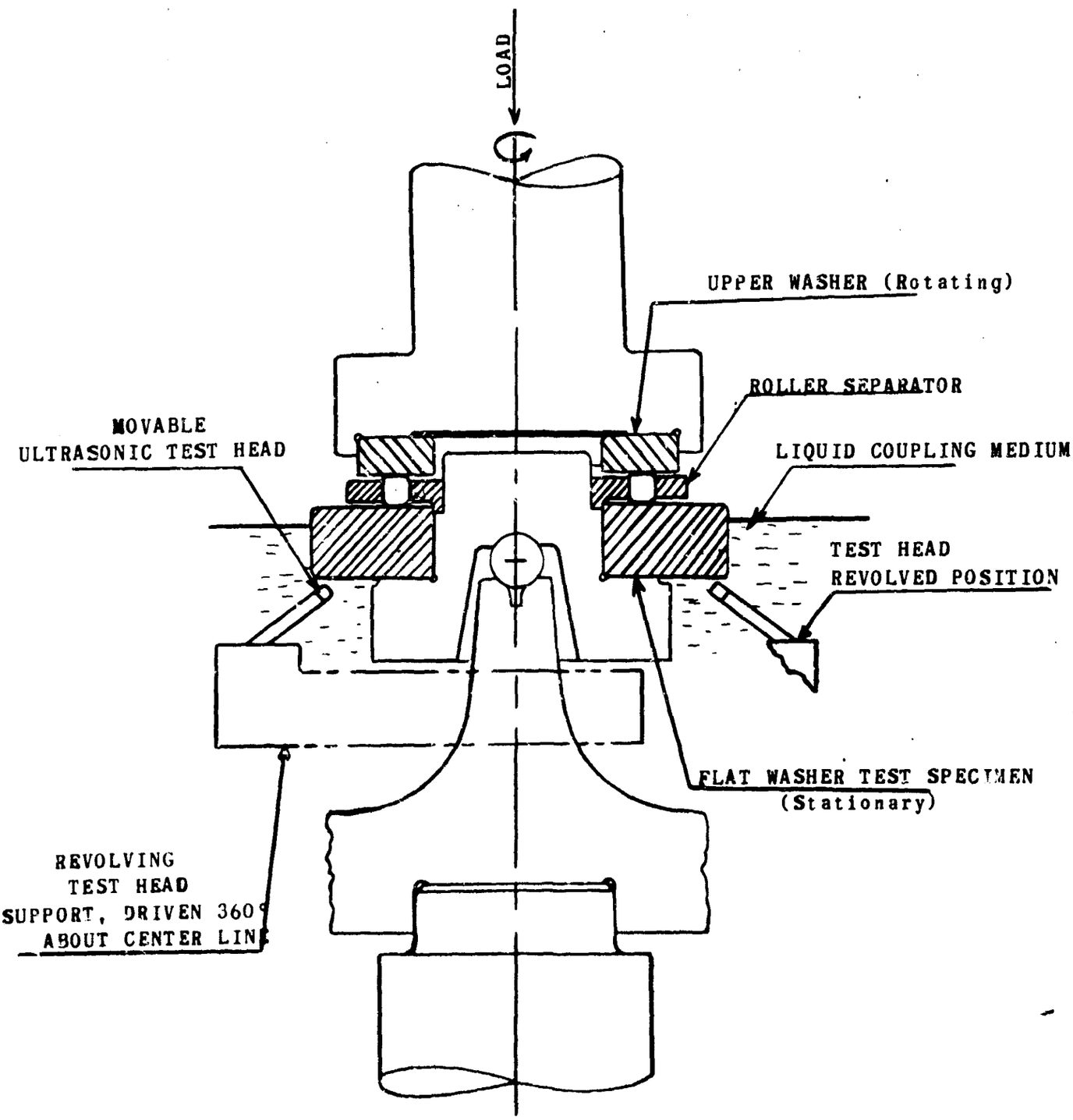

RESEARCH LABORATORY SKF INDUSTRIES, INC.

ENCLOSURE 31

SCHEMATIC OF ALFAX RECORDER CHART

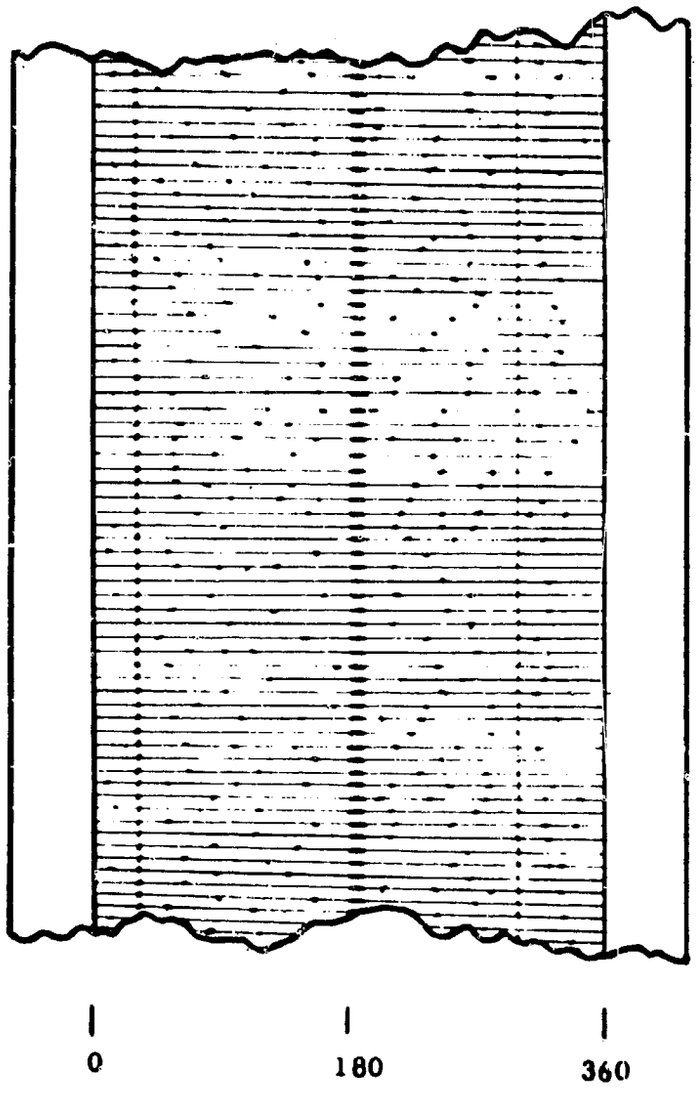

Legitimate defect indications are aligned vertically.

Random noise indications are not repeated at the same azimuth locations and do not line up vertically.

ENCLOSURE 32

AL67M050

SCHEMATIC SHOWING THE TYPICAL FEATURES OF SPALLS AND THE RELATIONSHIP BETWEEN CRACK PROPAGATION AND DEFORMATION BANDS

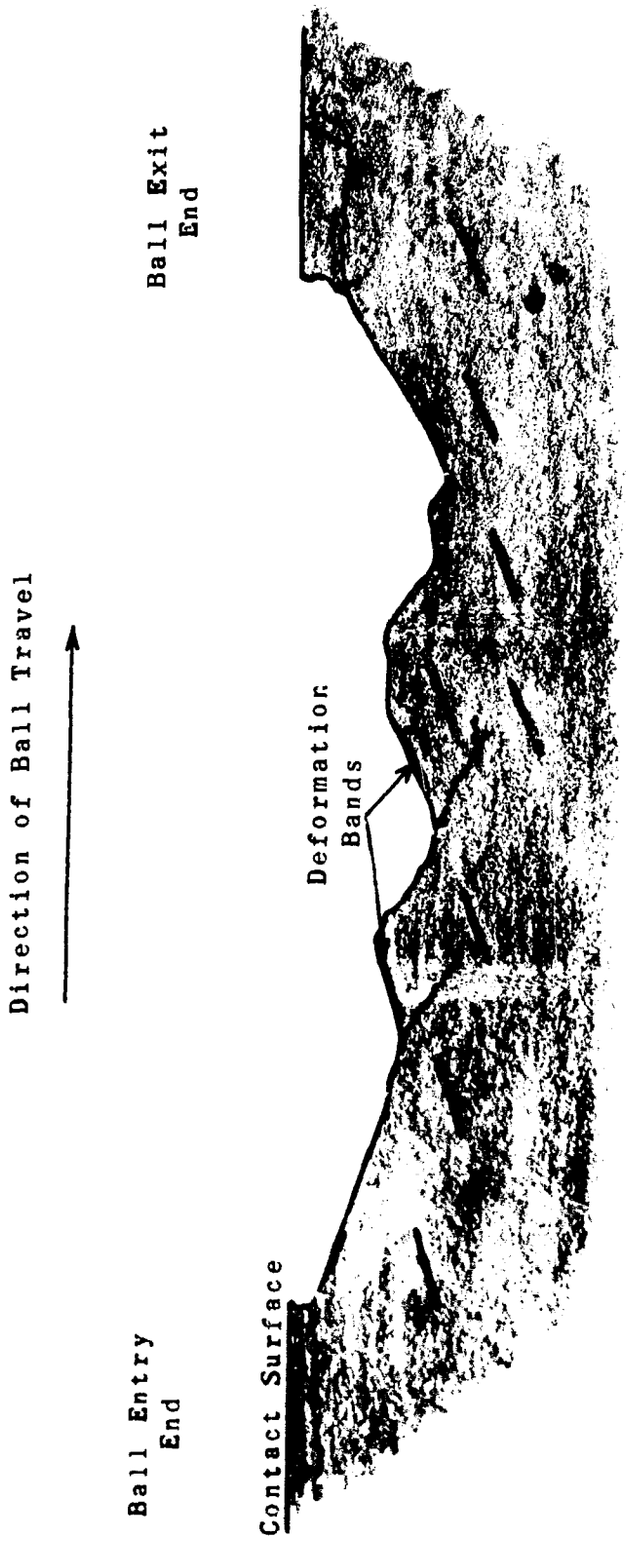

AL67M050

ENCLOSURE 33

SECTION THROUGH A SPALL SHOWING CRACK PROPAGATION ALONG DEFORMATION BANDS

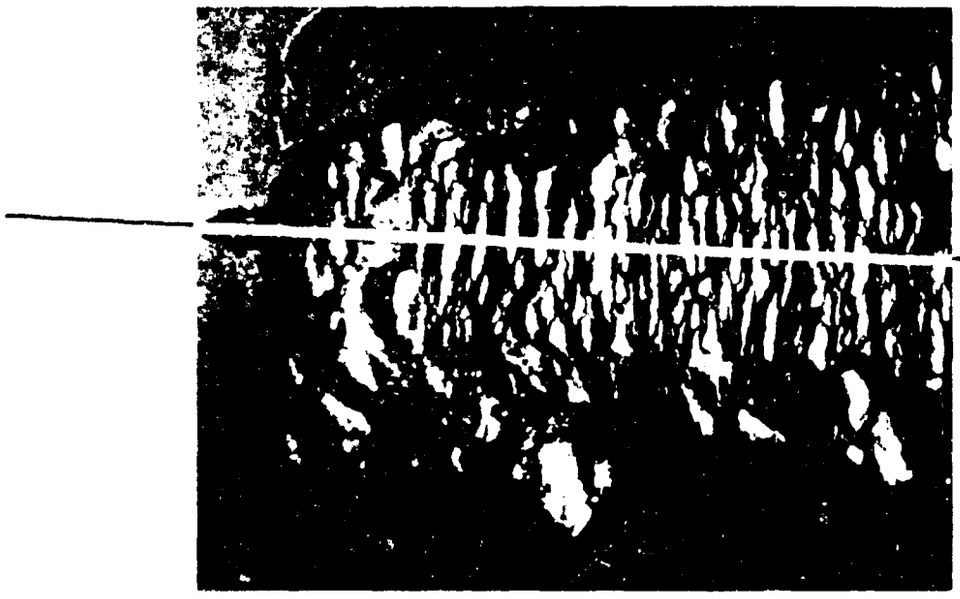

10X

Spalled surface showing cutting plane and furrow point of initiation.

Rolling Direction

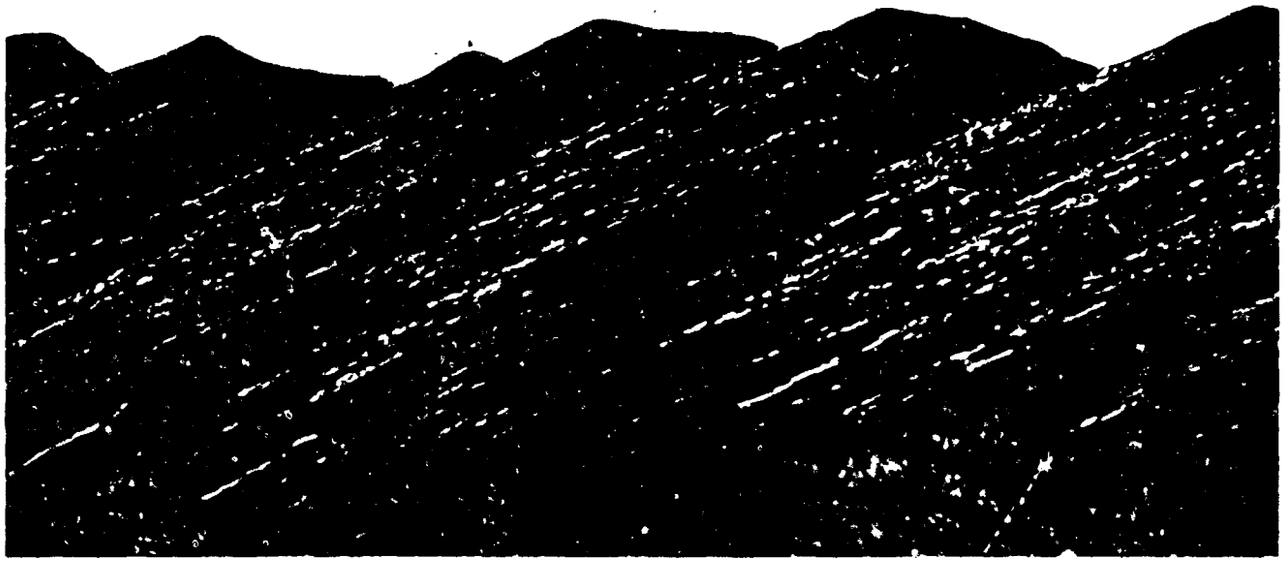

Circumferential cut made through the spall shows that the direction of crack propagation is dominated by the deformation bands. 200X

Security Classification

DOCUMENT CONTROL DATA - R&D

(Security classification of title, body of abstract and indexing annotation must be entered when the overall report is classified)

1. ORIGINATING ACTIVITY (Corporate author)	2a. REPORT SECURITY CLASSIFICATION
SKF Industries, Inc.	None
	2b. GROUP

3. REPORT TITLE

Third Summary Report on "Structural Studies of Bearing Steel Undergoing Cyclic Stressing"

4. DESCRIPTIVE NOTES (Type of report and inclusive dates)

5. AUTHOR(S) (Last name, first name, initial)

Martin, John A., Borgese, Salvatore, F, Eberhardt, Alvin D.

6. REPORT DATE	7a. TOTAL NO. OF PAGES	7b. NO. OF REFS
20 May 1967	74	20

8a. CONTRACT OR GRANT NO.	9a. ORIGINATOR'S REPORT NUMBER(S)
Nonr 4433 (00)	AL67M050
b. PROJECT NO. NR259-055/11-29-65	
c.	9b. OTHER REPORT NO(S) (Any other numbers that may be assigned this report)
d.	None

10. AVAILABILITY/LIMITATION NOTICES

11. SUPPLEMENTARY NOTES	12. SPONSORING MILITARY ACTIVITY
	Office of Naval Research

13. ABSTRACT

The microstructural changes seen in bearing steels after prolonged cyclic stressing are reviewed. It is shown that these changes arise from both plastic flow and the diffusion of carbon. The regions of plastic flow appear under the electron transmission microscope, as cell structures and under the light microscope as light etching bands, designated "deformation bands". Carbon diffusion is shown by the development of large carbides which grow during cycling. These are designated "lenticular carbides".

Microstructural alterations are seen as a bulk material phenomenon where the calculated shear stress exceeds an estimated threshold value of 120,000 psi. They also develop locally around stress raisers. It is shown that stress raisers severe enough to cause the growth of deformation bands are also frequently involved in the nucleation of fatigue failures. Sequences of photographs are shown which illustrate various stages of failure initiation at four types of microscopic defects: Debris dents, grinding furrows, surface pits of unknown origin, and non-metallic inclusions.

DD FORM 1 JAN 64 1473

Security Classification

Security Classification

14. KEY WORDS	LINK A		LINK B		LINK C	
	ROLE	WT	ROLE	WT	ROLE	WT
Rolling Contact Fatigue						
Microstructural Changes in Fatigue						
Surface Defects						
Bearing Fatigue						

INSTRUCTIONS

1. ORIGINATING ACTIVITY: Enter the name and address of the contractor, subcontractor, grantee, Department of Defense activity or other organization *(corporate author)* issuing the report.

2a. REPORT SECURITY CLASSIFICATION: Enter the overall security classification of the report. Indicate whether "Restricted Data" is included. Marking is to be in accordance with appropriate security regulations.

2b. GROUP: Automatic downgrading is specified in DoD Directive 5200.10 and Armed Forces Industrial Manual. Enter the group number. Also, when applicable, show that optional markings have been used for Group 3 and Group 4 as authorized.

3. REPORT TITLE: Enter the complete report title in all capital letters. Titles in all cases should be unclassified. If a meaningful title cannot be selected without classification, show title classification in all capitals in parenthesis immediately following the title.

4. DESCRIPTIVE NOTES: If appropriate, enter the type of report, e.g., interim, progress, summary, annual, or final. Give the inclusive dates when a specific reporting period is covered.

5. AUTHOR(S): Enter the name(s) of author(s) as shown on or in the report. Enter last name, first name, middle initial. If military, show rank and branch of service. The name of the principal author is an absolute minimum requirement.

6. REPORT DATE: Enter the date of the report as day, month, year; or month, year. If more than one date appears on the report, use date of publication.

7a. TOTAL NUMBER OF PAGES: The total page count should follow normal pagination procedures, i.e., enter the number of pages containing information.

7b. NUMBER OF REFERENCES: Enter the total number of references cited in the report.

8a. CONTRACT OR GRANT NUMBER: If appropriate, enter the applicable number of the contract or grant under which the report was written.

8b, &c, & 8d. PROJECT NUMBER: Enter the appropriate military department identification, such as project number, subproject number, system numbers, task number, etc.

9a. ORIGINATOR'S REPORT NUMBER(S): Enter the official report number by which the document will be identified and controlled by the originating activity. This number must be unique to this report.

9b. OTHER REPORT NUMBER(S): If the report has been assigned any other report numbers *(either by the originator or by the sponsor)*, also enter this number(s).

10. AVAILABILITY/LIMITATION NOTICES: Enter any limitations on further dissemination of the report, other than those imposed by security classification, using standard statements such as:

(1) "Qualified requesters may obtain copies of this report from DDC."

(2) "Foreign announcement and dissemination of this report by DDC is not authorized."

(3) "U. S. Government agencies may obtain copies of this report directly from DDC. Other qualified DDC users shall request through _____."

(4) "U. S. military agencies may obtain copies of this report directly from DDC. Other qualified users shall request through _____."

(5) "All distribution of this report is controlled. Qualified DDC users shall request through _____."

If the report has been furnished to the Office of Technical Services, Department of Commerce, for sale to the public, indicate this fact and enter the price, if known.

11. SUPPLEMENTARY NOTES: Use for additional explanatory notes.

12. SPONSORING MILITARY ACTIVITY: Enter the name of the departmental project office or laboratory sponsoring *(paying for)* the research and development. Include address.

13. ABSTRACT: Enter an abstract giving a brief and factual summary of the document indicative of the report, even though it may also appear elsewhere in the body of the technical report. If additional space is required, a continuation sheet shall be attached.

It is highly desirable that the abstract of classified reports be unclassified. Each paragraph of the abstract shall end with an indication of the military security classification of the information in the paragraph, represented as *(TS), (S), (C), or (U)*.

There is no limitation on the length of the abstract. However, the suggested length is from 150 to 225 words.

14. KEY WORDS: Key words are technically meaningful terms or short phrases that characterize a report and may be used as index entries for cataloging the report. Key words must be selected so that no security classification is required. Identifiers, such as equipment model designation, trade name, military project code name, geographic location, may be used as key words but will be followed by an indication of technical context. The assignment of links, rules, and weights is optional.

Security Classification